# Delayed activation of the DNA replication licensing system in Lgr5(+) intestinal stem cells

T.D. Carroll[1], I.P. Newton[1], Y. Chen[1], J.J. Blow*[2], I. Näthke*[1]

Affiliations: [1]Cell & Developmental Biology and [2]Centre for Gene Regulation and Expression, University of Dundee, Dundee, Scotland, UK, DD15EH
*Correspondence to: j.j.blow@dundee.ac.uk or i.s.nathke@dundee.ac.uk

**ABSTRACT**

During late mitosis and early $G_1$, replication origins are licensed for replication by binding to double hexamers of MCM2-7. Here, we investigate how licensing and proliferative commitment are coupled in the small-intestinal epithelium. We developed a method for identifying cells in intact tissue containing DNA-bound MCM2-7. Interphase cells above the transit-amplifying compartment had no DNA-bound MCM2-7, but still expressed MCM2-7 protein, suggesting that licensing is inhibited immediately upon differentiation. Strikingly, we found most proliferative Lgr5(+) stem cells are in an unlicensed state. This suggests that the elongated cell-cycle of intestinal stem-cells is caused by an increased $G_1$ length, characterised by dormant periods with unlicensed origins. Significantly, the unlicensed state is lost In *Apc* mutant epithelium, which lacks a functional restriction point, causing licensing immediately upon $G_1$ entry. We propose that the unlicensed $G_1$ of intestinal stem cells creates a temporal window when proliferative fate decisions can be made.

## INTRODUCTION

Cell division is necessary for adult tissue homeostasis. It allows for the replacement of aged or damaged cells and the provision of specialised cells critical for tissue function. The decision to proliferate is crucial, especially for stem cells, which produce daughter cells that either maintain a stem cell fate or differentiate to produce specialised cells. The rapidly-renewing intestinal epithelium replenishes its cellular content every 4-5 days. This high turnover rate is maintained primarily by Lgr5(+) intestinal stem cells in the crypt base, thought to be continually proliferative (Basak et al., 2014) as confirmed by proteomic and transcriptomic analysis (Munoz et al., 2012). There is also a quiescent stem cell-population that can re-engage with the cell-cycle to repopulate the Lgr5(+) cell population if it becomes depleted. These quiescent stem cells reside at the +4 position and constitute a subset of Lgr5(+) cells and are immature secretory lineage precursors (Buczacki et al., 2013). Lgr5(+) stem cells can divide to form transit-amplifying (TA) cells, which undergo several rounds of cell division before differentiating and losing proliferative competency (Potten and Loeffler, 1990).

How proliferative fate decisions are governed in stem cells and transit-amplifying cells is not understood. Lineage tracing studies suggest that in homeostatic intestinal tissue only 5-7 intestinal stem cells are ‘active’ out of the 12-16 Lgr5(+) cells present in the crypt base (Baker et al., 2014, Kozar et al., 2013). Interestingly, Lgr5(+) cells have a significantly longer cell-cycle than transit-amplifying cells (Schepers et al., 2011). The functional significance of the prolonged cell-cycle time of Lgr5(+) stem cells is currently unknown, but suggests active regulation of cell-cycle progression and proliferative fate commitment.

43 Proliferative fate decisions are typically visualised by detecting markers that are present in
44 all cell-cycle phases, and only distinguish proliferative from quiescent cells. Visualising the
45 incorporation of labelled nucleosides such as BrdU or EdU marks cells in S-phase. The
46 limitation of these methods is that they cannot discriminate early proliferative fate
47 decisions made during the preceding mitosis, or in the early stages of $G_1$. DNA replication in
48 S phase depends on origin licensing, involving the regulated loading of minichromosome
49 maintenance 2-7 (MCM2-7) complexes onto origins of DNA replication (reviewed in (Blow
50 and Hodgson, 2002, Champeris Tsaniras et al., 2014)). During S phase, DNA-bound MCM2-7
51 hexamers are activated to form the catalytic core of the DNA helicase as part of the CMG
52 (Cdc45, MCM2-7, GINS) complex (Moyer et al., 2006, Ilves et al., 2010, Makarova et al.,
53 2012). Replication licensing is thought to occur from late mitosis throughout $G_1$ until
54 passage through the restriction point (Dimitrova et al., 2002, Haland et al., 2015, Namdar
55 and Kearsey, 2006, Symeonidou et al., 2013). Correspondingly, insufficient origin licensing
56 directly limits the ability to progress past the restriction point causing cell cycle arrest (Alver
57 et al., 2014, Liu et al., 2009, Shreeram et al., 2002). When functional, this licensing-
58 checkpoint can delay S-phase if an insufficient amount of origins have been licensed.

59 When cells enter $G_0$, MCM2-7 proteins are downregulated and degraded, primarily via E2F-
60 mediated transcriptional control of MCM2-7, Cdc6 and Cdt1 (Leone et al., 1998, Ohtani et
61 al., 1999, Williams et al., 1998). This prevents terminally differentiated cells from re-entering
62 the cell cycle. In mammalian cells, artificial induction of quiescence through contact
63 inhibition leads to gradual downregulation of Cdc6 and MCM2-7 over several days
64 (Kingsbury et al., 2005). These features have led to the suggestion that quiescence can be
65 defined by an unlicensed state (Blow and Hodgson, 2002). Equally, the licensing status can

66 define a different restriction point that signals proliferative fate commitment at the end of
67 mitosis and in early $G_1$, independently of the Rb/E2F restriction point.

68 The dynamics of replication licensing in the intricate cellular hierarchy of a complex, rapidly
69 renewing adult tissue, is not understood. Therefore, we investigated the licensing system in
70 the intestinal epithelium, aiming to understand dynamics of early cell-cycle commitment in
71 stem and transit-amplifying cells and during terminal differentiation.

72 **MATERIALS AND METHODS**

73 **Mice**

74 All experiments were performed under UK home office guidelines. CL57BL/6 (Wild-type),
75 *R26-rtTA Col1A1-H2B-GFP* (H2B-GFP), Lgr5-EGFP-IRES-creERT2 ($Lgr5^{GFP/+}$) and $Apc^{Min/+}$ mice
76 were sacrificed by cervical dislocation or $CO_2$ asphyxiation. Fucci2aR mice (Mort et al., 2014)
77 were a kind gift of Dr Richard Mort, University of Edinburgh.

78 **Tissue preparation: Whole small intestine**

79 Dissected pieces of adult mouse small-intestine were washed briefly in PBS and then fixed in
80 4% PFA for 3 hours, 4°C. Intestines were cut into 2x2 $cm^2$ pieces and fixed overnight in 4%
81 PFA, 4°C. Tissue was embedded in 3% low melting temperature agarose and cut into 200 µm
82 sections using a Vibratome (Leica). Sections were washed in PBS, permeabilised with 2%
83 Triton-X100 for 2 hours and incubated with Blocking Buffer (1% BSA, 3% Normal Goat
84 serum, 0.2% Triton-X100 in PBS) for 2 hours, 4°C. Tissue was incubated in Working Buffer
85 (0.1% BSA, 0.3% Normal Goat Serum, 0.2% Triton-X100 in PBS) containing primary antibody,
86 Mcm2 (Cell Signalling, 1:500), for 48 hours, 4°C. Sections were washed 5x with Working

87 Buffer prior to 48 hour incubation with secondary antibodies diluted in Working Buffer:
88 Alexafluor™ conjugated goat anti-rabbit (1:500, Molecular Probes) plus 5 µg/ml Hoechst
89 33342 and Alexafluor™ conjugated Phalloidin (1:150, Molecular Probes). Sections were
90 mounted on coverslips in Prolong Gold between 2x120 µm spacers.

91 **Tissue preparation:**

92 **Isolating and staining crypts**

93 Small intestines were dissected, washed in PBS and opened longitudinally. Villi were
94 removed by repeated (up to 10 times) scraping of the luminal surface with a coverslip.
95 Tissue was washed in PBS, incubated in 30 mM EDTA (25 minutes, 4°C) and crypts isolated
96 by vigorous shaking in PBS. Crypt suspensions were centrifuged (fixed rotor, 88 RCF, 4°C)
97 and the pellet washed twice in cold PBS. Crypts were fixed in 4% PFA (30min, room
98 temperature), permeabilized in 1% Triton-X100 (1 hour, room temperature) and blocked in
99 Blocking Buffer (2 hours, 4°C). Crypts were incubated with primary antibodies diluted in
100 Working Buffer: Mcm2 (Cell Signalling, 1:500), phospo-HistoneH3 (Abcam, 1:500), Ki67
101 (Abcam ab15580, 1:250), αGFP (Abcam, 1:500), washed 5x with Working Buffer before
102 overnight incubation with secondary antibodies diluted in Working buffer: Alexafluor™
103 conjugated goat anti-mouse or anti-rabbit (1:500, Molecular Probes) or stains: Rhodamine
104 labelled Ulex Europaeus Agglutinin I (UEA, 1:500), 5 µg/ml Hoechst 33342 or Alexafluor™
105 conjugated Phalloidin (1:150), at 4°C. Crypts were mounted directly on slides in Prolong
106 Gold, overnight.

107 **CSK extraction of isolated crypts**

108 Soluble proteins were extracted from crypts isolated as described above by incubation with
109 CSK extraction buffer (10 mM HEPES, 100 mM NaCl, 3 mM $MgCl_2$, 1 mM EGTA, 300 mM
110 sucrose, 0.2% TritonX-100, 1 mM DTT, 2% BSA) supplemented with protease inhibitors
111 (PMSF, Pepstatin, Leupeptin, Cystatin, $Na_3VO_4$, NaF, aprotinin) for 20 minutes on ice prior to
112 fixation. Crypts were then fixed with 4% PFA and processed for imaging as described above.

113 **H2B-GFP label retention**

114 H2B-GFP expression in transgenic *R26-rtTA Col1A1-H2B-GFP* mice was induced by replacing
115 normal drinking water with 5% sucrose water supplemented with 2 mg/ml doxycycline.
116 After 7 days, doxycycline water was replaced with normal drinking water. Subsequently,
117 mice were sacrificed after 7 days.

118 **EdU incorporation and detection**

119 Mice were injected intraperitoneally with 100 µg EdU (Invitrogen) prepared in 200 µl sterile
120 PBS. Mice were sacrificed 1 hour or 17 hours post induction. For organoids, 10 µM EdU was
121 included in crypt media for 1 hour before harvesting. EdU was detected by Click-it
122 chemistry, by incubation in EdU working buffer (1.875 µM Alexafluor 488 azide (Invitrogen),
123 2 mM $CuSO_4$, 10 mM Ascorbic acid), overnight at 4°C, prior to processing for
124 immunofluorescence staining.

125 **Organoid Culture**

126 Isolated crypts were dissociated to single cells with TripLE express (Life Technologies) at
127 37°C, 5 minutes. Dissociated cells were filtered through a 40 µm cell strainer (Greiner) and

128 suspended in growth factor reduced Matrigel (BD Biosciences). Organoids were grown in
129 crypt media (Advanced DMEM/F12 (ADF) supplemented with 10 mM HEPES, 2 mM
130 Glutamax, 1 mM N-Acetylcysteine, N2 (Gemini), B27 (Life technologies),
131 Penicillin/Streptomycin (Sigma) supplemented with growth factors – ENR media (EGF (50
132 ng/ml, Invitrogen), Noggin (100 ng/ml, eBioscience) and RSpondin conditioned media
133 produced from stably transfected L-cells (1:4). Chiron99021 (3 µM), Valproic acid (1 mM,
134 Invitrogen) and Y27632 (10 µM, eBiosciences) were added to the culture for the first 48
135 hours. Organoids were passaged every 3-5 days by mechanically disrupting Matrigel and by
136 washing and pipetting in ADF. Dissociated crypts were re-suspended in fresh Matrigel and
137 grown in crypt media supplemented with growth factors.

138 For small molecule treatments, primary intestinal epithelial cells were cultured in ENR-CVY
139 (ENR plus Chiron99021, Valproic acid and Y27632) for 3 Days, and then organoids were sub-
140 cultured in ENR for two further days prior to the start of the experiment. Organoids were
141 then treated with the stated small molecules for the indicated time periods. For induction of
142 Unlicensed-$G_1$, organoids were treated with Gefitinib (5 µM) coupled with removal of EGF
143 from the crypt media. For re-activation/chase period, the media was removed and fresh
144 growth factors added. All growth factors and inhibitors were replenished every 2 days
145 throughout the experiment.

146 **Flow cytometry and cell sorting**

147 Intestinal crypts were isolated and dissociated to single cells as described above. Isolated
148 cells were filtered through 40 µm cell strainers (Greiner). For organoids, following one PBS
149 wash, organoids were dissociated to single cells by incubation in TripLE express for 15

150 minutes at room temperature followed by manual disruption by pippetting. Cells were then
151 extracted with CSK buffer for 20 minutes on ice, followed by fixation in 0.5% PFA (pH7.40,
152 15 minutes, room temperature). Cells were then washed once in 1% BSA and permeabilized
153 with ice-cold 70% EtOH, 10 minutes. Cells were then washed in 1% BSA and re-suspended
154 with primary antibodies (Mcm2, 1:500; GFP, 1:500; Ki67, 1:200) diluted in Working buffer
155 (overnight, 4°C). Following two washes in working buffer, cells were re-suspended in
156 secondary antibodies goat anti-mouse or anti-rabbit (Alexafluor647, 1:500 (Molecular
157 Probes); Alexafluor488-Ki67, 1:400 (Clone SolA15, BD Biosciences), diluted in working buffer
158 (1 hour, room temperature). After two washes in 1% BSA, cells were suspended in working
159 buffer containing 15 µg/ml DAPI. Samples were analysed on a FACS Canto (BD Biosciences).

160 For cell sorting, cells were isolated from Lgr5-GFP mice as described above by treatment
161 with TripLE express for 15 minutes, 37°C followed by filtration through 40 µm filters
162 (Greiner). Cells were sorted in ADF supplemented with 1% FBS and DAPI (15 µg/ml). Sorting
163 was performed using an Influx™ Cell sorter (BD biosciences). Cells were checked post-sort
164 to ensure sample purity by re-examining Lgr5 expression in the sorted gates.

165 **Microscopy and Image analysis**

166 Samples were imaged using a Zeiss LSM 710 microscope using a 40X LD Pan-Neofluar
167 objective lens and immersion oil with a refractive index of 1.514. Z-stacks were acquired at
168 optimal section intervals between 0.3 and 0.8 µm. For quantification, images were acquired
169 at 16 bit-depth.

170 Image processing and analysis were performed using Imaris (Bitplane). Images of individual
171 crypts were manually cropped, ensuring that an individual crypt was the only region of

172 interest. All nuclei were detected in individual crypts using automated thresholding in Imaris
173 using the measurement point function, set to detect nuclei at an estimated size of 3.5 µm.
174 Missed or incorrectly assigned nuclei were manually identified. This function produced
175 measurement points that segmented the specific region at the corresponding co-ordinate of
176 the measurement point. Mean intensities for different channels were calculated per spot.
177 This equates to the intensity at the centre region of each nucleus. A reference nucleus at the
178 crypt base was used to define the crypt base position. The Euclidean distance to this point
179 was measured and defined as the distance to the crypt base. Multiple images were analysed
180 using the same workflow and the analysed files collated. For vibratome sections, a plane
181 was manually defined running through to the muscle layer beneath the epithelium. The
182 smallest distance to this surface was defined for segmented nuclei. For nuclear volume
183 estimation, nuclei were manually segmented in 3D using the manual segmentation tools
184 within Imaris (**S1 Figure**).

185 **Flow cytometry analysis**

186 Flow cytometry data was analysed using FlowJo (Treestar) using a standardised gating
187 strategy (**S1 Figure**). Briefly, cells were identified using FSC and SSC. Following doublet
188 discrimination, gates were set using appropriate controls lacking conjugated secondary
189 antibodies and without primary antibodies. Mcm2 negative gates were set by secondary
190 only controls in conjunction with the Mcm2 intensity of $G_2$ cells. $G_1$ cells were discriminated
191 based on the maximal DNA-bound Mcm2 intensity prior S-phase, and by DAPI intensity.

192 **Computational Modelling**

193 A deterministic computer model for licensing in G1 was written in the Swift programming
194 language using the Xcode 9 development environment. The model assumes that there is a
195 minimum G1 period that is required for cells to grow to a critical size before they can enter S
196 phase. Licensing can take place during this period at a constant rate. A licensing rate of 1
197 means that cells will be fully licensed in exactly the minimum G1 period. It is also assumed
198 that cells have a robust 'licensing checkpoint' (Shreeram et al., 2002, Blow and Gillespie,
199 2008) so that they cannot enter S phase until origins have been fully licensed. An optional
200 'unlicensed G1 period' occurs at the start of G1, during which time no licensing takes place.
201 In the simulation, cells enter G1, wait for any optional 'unlicensed G1 period', then start to
202 license origins at a fixed rate; cells exit G1 and modelling ceases only when they have
203 become maximally licensed and also the minimum G1 period has elapsed. The model divides
204 the minimum G1 period into 10,000 equal steps and records the degree of licensing at the
205 end of each step in the 'Licensing Array'. The contents of the Licensing Array are distributed
206 into 101 different frequency bins, ranging from 0% (no licensing) to 100% (maximal
207 licensing). To model the background signal recorded by flow cytometry, all the licensing

values are increased by 5%. To model flow cytometry measurement error, the frequency array is smoothed by starting at the smallest bin and pushing 80% of the cell counts into the next largest bin, and then starting at the largest bin pushing 80% of the cell counts into the next smallest bin.

```
//
//  JBLicensingRateModel.swift version 1.0
//
//  Created by Julian Blow on 05/10/2017.


import Foundation

class JBLicensingRateModel {
    let licensingRate: Double    // rate of licensing in proportion to minimum G1 length
    let proportionUnlicensedG1: Double      // proportion of minimum G1 before licensing occurs
    let timeStepsForMinimumG1: Int
    let licensingPerStep: Double
    let timeStepsBeforeLicensingStarts: Int
    let binsForFACS: Int
    let backgroundForFACS: Double
    let binSmoothingProportion: Double
    let totalNumberOfCells: Double
    let precisionCutOffForSmoothing: Double
    let numberOfTimepointsOutput: Int

    init (licensingRate: Double, proportionUnlicensedG1: Double) {
        self.licensingRate = licensingRate
        self.proportionUnlicensedG1 = proportionUnlicensedG1
        timeStepsForMinimumG1 = 10000
        licensingPerStep = (licensingRate / Double(timeStepsForMinimumG1)) * 100
        timeStepsBeforeLicensingStarts = Int(proportionUnlicensedG1 * Double(timeStepsForMinimumG1))
        binsForFACS = 100
        backgroundForFACS = 5
        binSmoothingProportion = 0.8
        totalNumberOfCells = 10000.0
        precisionCutOffForSmoothing = totalNumberOfCells / 10000     // cutoff for the smallest number of cells we continue to
smooth for the far right of the array
        numberOfTimepointsOutput = 100
    }

    func run () -> ([Double], [Double])  {
        var licensingTimepoints: [Double]
        if licensingRate > 0 { licensingTimepoints = simulateLicensing() }
        else { licensingTimepoints = Array(repeating: 0.0, count: timeStepsForMinimumG1) }       // if licensing can never occur
        let FACSOutputExact = simulateFACSExact(licensingTimepoints: licensingTimepoints)
        let FACSOutput = smoothFACSOutput(FACSOutputExact: FACSOutputExact)
        var simplifiedLicensingTimepoints = [Double]()
        for index in stride(from: 0, to: licensingTimepoints.count, by: licensingTimepoints.count/numberOfTimepointsOutput) {
            simplifiedLicensingTimepoints.append(licensingTimepoints[index])
        }
        return (FACSOutput, simplifiedLicensingTimepoints)
    }

    func simulateLicensing() -> [Double] {
    // simulates the degree of MCM loading given the licensingRate and proportionUnlicensed
    // returns amount of MCM loaded (percent max) at different time points
        var amountOfLicensing = 0.0
        var licensingArray = Array(repeating: 0.0, count: timeStepsBeforeLicensingStarts)
        var timeStep = timeStepsBeforeLicensingStarts

        repeat {
            amountOfLicensing += licensingPerStep
            if amountOfLicensing > 100 { amountOfLicensing = 100 }
            licensingArray.append(amountOfLicensing)
```

```
272             timeStep += 1
273         } while (amountOfLicensing < 100) || (timeStep < timeStepsForMinimumG1)
274
275         return licensingArray
276     }
277
278     func simulateFACSExact (licensingTimepoints: [Double]) -> [Double] {
279     // takes an array amount of MCM loaded at different time points as created by simulateLicensing()
280     // turns this into a simulated output from a FACS (flow cytometry) analysis with totalNumberOfCells
281         var maxMCMValue = licensingTimepoints.max()! // can be >100 because of smoothing
282         if maxMCMValue == 0 { maxMCMValue = 100 }      // if no licensing occurred
283         var FACSOutputExact = Array(repeating: 0.0, count: binsForFACS+1)        // binsForFACS+1 because we 0 and 100 are
284 both possible
285         let numberOfCellsPerTimepoint = totalNumberOfCells / Double(licensingTimepoints.count)              // so we get
286 totalNumberOfCells events
287         for anMCMContent in licensingTimepoints {
288             let binIndex = Int(anMCMContent * Double(binsForFACS) / maxMCMValue)
289             assert(binIndex <= binsForFACS, "Cannot have an MCM content greater than 100, the bin number")
290             if binIndex>=0 { FACSOutputExact[binIndex] += numberOfCellsPerTimepoint }                    // add cells to bin
291         }
292
293         return FACSOutputExact
294     }
295
296     func smoothFACSOutput (FACSOutputExact: [Double]) -> [Double] {
297         // simulates the error in FACS data by:
298         // first adding a background of backgroundForFACS to all samples
299         // then pushing binSmoothingProportion of each bin into the higher bin, when the value > cutOffForDither
300         // then pushing binSmoothingProportion of each bin into the lower bin
301         let backgroundBins = Array(repeating: 0.0, count: Int(backgroundForFACS))
302         var FACSOutput = backgroundBins + FACSOutputExact          // add the background of empty pbins
303         var binIndex = 0
304         var amountToShift = 0.0
305        repeat {                        // expand rightwards by dithering
306             amountToShift = FACSOutput[binIndex] * binSmoothingProportion
307             FACSOutput[binIndex] -= amountToShift
308             if binIndex+1 < FACSOutput.count { FACSOutput[binIndex+1] += amountToShift }
309             else { FACSOutput.append(amountToShift) }
310             binIndex += 1
311             }   while   (amountToShift   >=   precisionCutOffForSmoothing)   ||   (binIndex   <   FACSOutputExact.count   +
312 Int(backgroundForFACS))
313
314        binIndex = FACSOutput.count-1
315         while binIndex >= 0 {                  // expand leftwards by dithering
316             amountToShift = FACSOutput[binIndex] * binSmoothingProportion
317             FACSOutput[binIndex] -= amountToShift
318             if binIndex > 0 { FACSOutput[binIndex-1] += amountToShift }
319             binIndex -= 1
320         }
321
322         return FACSOutput
323     }
324
325 }
```

326 **RESULTS**

327 **Mcm2 expression declines along the crypt-villus axis**

328 Because of their abundance, strong conservation and association with the core DNA
329 replication process, the presence of MCM2-7 proteins is commonly used to establish
330 proliferative capacity in tissues, similar to Ki67 or PCNA (Gonzalez et al., 2005, Jurikova et

331 al., 2016, Stoeber et al., 2001, Williams et al., 1998). Usually, terminally differentiated cells
332 in mammalian tissues do not contain MCM2-7 (Stoeber et al., 2001, Todorov et al., 1998,
333 Eward et al., 2004). To establish the overall MCM2-7 protein abundance along intestinal
334 crypts, we first examined the expression of MCM2-7 proteins in adult murine small-
335 intestinal epithelium using high-resolution immunofluorescence microscopy. We focused on
336 Mcm2 as a surrogate for all the members of the MCM2-7 complex based on their similar
337 function and localisation. However, we repeated a subset of the experiments using an
338 antibody to Mcm4, which is less effective in detecting endogenous proteins. Nonetheless, in
339 all cases, the results were identical.

340 Consistent with previous reports, Mcm2 was highly expressed in both murine and human
341 intestinal epithelium. Mcm2 was highly expressed in intestinal crypts (**Figure 1A**) and
342 declined gradually along the crypt-villus axis (**Figure 1B**), but persisted in a few cells in the
343 villus compartment (**Figure 1D**). Mcm2 was nuclear in interphase cells but cytoplasmic
344 during mitosis (**Figure 1C**). Although the majority of intestinal crypt cells expressed Mcm2,
345 at the crypt base, Mcm2(+) and Mcm2(-) cells were interspersed (**Figure 1A, D**), consistent
346 with previous reports (Pruitt et al., 2010). This pattern is reminiscent of the alternating
347 arrangement of Lgr5(+) stem cells and Paneth cells at the crypt base (Barker et al., 2007).
348 Lgr5(+) stem cells express Ki67 and are continually proliferative whereas Paneth cells are
349 fully differentiated and are Ki67(-) (Basak et al., 2014). As expected, Mcm2 was expressed in
350 all Lgr5(+) stem cells and there was a strong correlation between Mcm2 and Lgr5 expression
351 (**Figure 1E**). This is consistent with the idea that Lgr5$^{Hi}$ stem cells are the main proliferative
352 stem cells in the intestinal crypt. Staining with Ulex Europaeus Agglutinin I (UEA),
353 demonstrated that most Mcm2(-) cells in the crypt base are UEA(+) Paneth cells (**Figure 1F**).

354 Normally, MCM2-7 expression is lost in terminally differentiated cells (Eward et al., 2004,
355 Stoeber et al., 2001, Williams et al., 1998, Williams et al., 2004). The loss of expression has
356 been suggested as a major contributor to the proliferation-differentiated switch *in vivo.* To
357 test this idea, we measured the Mcm2 content of young and mature secretory cells in
358 intestinal crypts and villi (**Figure 1G, H**). There was differential expression of Mcm2 in
359 distinct secretory lineages. Many mature secretory cells including Paneth, Goblet and
360 enteroendocrine cells were Mcm2(-), consistent with their differentiation status and long
361 life-span in the epithelium (van der Flier and Clevers, 2009). We detected a small number of
362 UEA(+) Mcm2(+) cells in intestinal crypts (**Figure 1G**). Assuming that Mcm2 expression
363 declines slowly after terminal differentiation, the presence of Mcm2 in UEA(+) secretory
364 cells could reflect their immaturity. Consistently, Mcm2 expression in UEA(+) cells in crypts
365 was significantly higher than in villi (**Figure 1H**), supporting the idea that MCM2-7 are
366 gradually lost upon terminal differentiation. Since MCM2-7 are highly abundant and have a
367 long (>24 hour) half-life (Musahl et al., 1998), it likely that after cells differentiate, their
368 MCM2-7 content declines at a slow rate, explaining why Mcm2 persists in the villus
369 compartment.

370 **Visualisation of DNA replication licensing *In vivo***

371 MCM2-7 exist in three states: as hexamers free in the nucleoplasm, as double hexamers
372 bound to DNA during late mitosis, G1 and S phase, or as CMG complexes at replication forks
373 during S phase (Evrin et al., 2009, Gambus et al., 2011, Remus et al., 2009). To distinguish
374 between DNA-bound and soluble forms, we developed a protocol involving a brief
375 extraction of isolated crypts with non-ionic detergent to remove soluble MCM2-7. The

376 remaining Mcm2 should mark cells whose origins are licensed for replication. Extraction did
377 not visibly affect intestinal crypt integrity but made them more opaque compared to
378 unextracted tissue (**Figure 2A**). The majority of cells in unextracted crypts were Mcm2(+)
379 (**Figure 2B,** 'Total') similar to tissue sections and mirroring the ubiquitous expression of Ki67
380 along the crypt axis. After extraction, the majority of the Mcm2 content in cells was lost
381 (**Figure 2B**, 'Licensed'), with only 10-30% of cells maintaining high levels of Mcm2 (**Figure**
382 **2C**). After extraction, Mcm2(+) was not present in mitotic cells expressing phosphorylated
383 histone H3, confirming the extraction procedure successfully removed non-DNA bound
384 MCM2-7 proteins (**Figure 2D**).

385 We used flow cytometry to measure MCM2-7 content more directly and further confirm the
386 effectiveness of the extraction procedure. Whereas the majority of isolated epithelial cells
387 expressed Mcm2 that persisted throughout the cell-cycle, extraction revealed a distinct
388 profile of Mcm-containing cells in crypts (**Figure 2E**). These profiles are consistent with those
389 reported for cultured cell lines (Friedrich et al., 2005, Haland et al., 2015, Moreno et al.,
390 2016, Matson et al., 2017). Mcm2 is present throughout the cell cycle (**Figure 2E**,
391 'Unextracted'), but extraction shows that it binds to DNA throughout $G_1$, reaching a
392 maximum level before cells enter S-phase, and is subsequently displaced from DNA during S
393 phase. This behaviour, which matches the known cell cycle behaviour of MCM2-7, confirms
394 the efficiency of our extraction protocol. An antibody against Mcm4 produced similar results
395 (data not shown). We observed that the majority of cells with a G1 DNA content appeared
396 to be unlicensed, having a DNA-bound Mcm2 content similar to $G_2$/M cells (**Figure 2E, E'**).
397 This is substantially different from typical profiles observed in cultured cells lines in which
398 most $G_1$ cells are fully licensed (Friedrich et al., 2005, Haland et al., 2015, Moreno et al.,

399 2016, Matson et al., 2017). Similar results were observed in cells isolated from intestinal
400 organoids (**Figure 2F, G**).

401 **Licensing status and cell-cycle progression along the crypt-villus axis**

402 Cell-cycle dynamics of intestinal stem and progenitor cells are highly heterogeneous (Pruitt
403 et al., 2010). The majority of Lgr5(+) stem cells are considered to be continually
404 proliferative, but with a much longer cell-cycle than transit-amplifying progenitor cells,
405 which are most commonly found in S-phase (Schepers et al., 2011). To investigate
406 proliferative fate decisions of intestinal epithelial cells, we used our MCM2-7 extraction in
407 crypts where S phase cells were labelled in vivo with the nucleoside analogue EdU. We then
408 used image analysis software to correlate Mcm2 content with cell-cycle stage along the
409 crypt-villus axis (**S1 Figure A-F**). This allowed quantification of licensing in relation to the
410 cell-cycle and 3D spatial information.

411 Figure 3A shows tissue labelled in vivo with a 1 hour EdU pulse followed by extraction of
412 soluble MCM2-7. As expected, the majority of cells in the transit-amplifying compartment
413 were labelled with EdU suggesting that most cells were in S-phase, consistent with early
414 studies using BrdU and [$^3$H]-thymidine labelling (Chwalinski and Potten, 1987). The patterns
415 of replication foci were consistent with the reported S-phase replication timing programme
416 (Rhind and Gilbert, 2013). Typically, all licensed cells had intense nuclear Mcm2 staining.
417 Some cells completely lacked Mcm2 and EdU labelling, suggesting they were in either $G_0$,
418 very early $G_1$ or in $G_2$. Some cells were labelled with both Mcm2 and EdU. These double-
419 labelled cells typically showed patterns of EdU labelling consistent with early to mid S phase
420 and Mcm2 labelling of DNA compartments expected to replicate later in S phase. This

421 relationship has been observed in tissue culture cells (Krude et al., 1996) and is consistent
422 with the idea that DNA-bound MCM2-7 are displaced from chromosomal domains as
423 replication is completed. Cells with late S-phase patterns of EdU labelling had little or no
424 detectable Mcm2, consistent with the displacement of the majority of MCM2-7 by the end
425 of S phase. We also measured nuclear volume, which increases during S phase and $G_2$. This
426 showed that nuclear volume increased up to two-fold in cells classified as S-phase and Late-
427 S/$G_2$ by Mcm2 and EdU staining (**Figure 3B)**. This confirms our cell-cycle assignment and also
428 suggests that most Mcm2(-) cells are in $G_0$ or $G_1$, rather than in $G_2$.

429 The combination of concurrently labelling DNA-bound Mcm2 and EdU showed a clear
430 correlation between cell position and cell-cycle stage. As noted previously, Mcm2 is
431 expressed in cells throughout the crypt (**Figure 3C, D**). At the base of the crypt, unlicensed
432 cells predominate (**Figure 3C, E**). At increasing distances from the crypt base there is a
433 successive rise in licensed $G_1$ cells, early/mid S phase cells and then late S/$G_2$ cells. Further
434 up the crypt, at the end of the TA compartment, these cell cycle stages decline in reverse
435 order, until unlicensed cells again predominate. This suggests that there is a co-ordinated
436 progression through the cell division cycle as cells enter, then leave, the TA compartment.
437 This was also observed as a field effect with many neighbouring cells showing similar
438 replication patterns (**S2 Figure A, B; S1 Movie**).

439 **Terminal differentiation is associated with a binary licensing decision**

440 At the terminal boundary of the transit-amplifying compartment, the majority of cells were
441 unlicensed and had no DNA-bound Mcm2 (**Figure 3C, E**). Similarly, there were no licensed $G_1$
442 cells beyond the TA compartment as defined by incorporation of EdU (**Figure 3F**). However,

443 total Mcm2 expression extended significantly beyond the last cells with DNA-bound Mcm2
444 or incorporated EdU (**Figure 3C, D, F**). The distribution of total Mcm2 expression
445 corresponded to the zone where cells express Ki67 (**S3 Figure**). Although Mcm2 and Ki67
446 expression persists beyond the TA compartment, licensing does not occur in this area. This
447 suggests that differentiation is not governed by a gradual reduction in total MCM2-7 levels,
448 but is a binary decision and licensing is abolished immediately after the final mitosis
449 preceding differentiation. To further examine this, we marked the terminally differentiated
450 zone by a 1 hour EdU pulse, followed by a 16 hour chase (**Figure 3G, H**). After 16 hours, the
451 majority of the distal end of the TA compartment became labelled with EdU. All labelled
452 nuclei in this area were significantly smaller than EdU(+) cells at the proximal end of the TA
453 compartment (data not shown), suggestive of their differentiation status. Importantly the
454 EdU(+) differentiated cells at the distal end of the TA compartment lacked DNA-bound
455 Mcm2, supporting our suggestion that licensing is inhibited immediately at terminal
456 differentiation.

457 **The majority of Intestinal stem cells spend the majority of $G_1$ in an unlicensed state**

458 The majority of cells in the crypt base expressed Mcm2, consistent with the finding that all
459 Lgr5(+) cells express Mcm2 but mature secretory cells, such as Paneth cells, do not (**Figure**
460 **1D, E**). Surprisingly, extraction revealed that only 7-15% of cells were licensed in the crypt
461 base (**Figure 3C, D**), with most cells in an unlicensed state despite expressing Mcm2. The
462 abundance of licensed cells peaked 40-60 µm away from the crypt base, corresponding to
463 just above the +4/+5 cell position (**Figure 3D, E**). This suggests that the majority of stem cells

464 remain unlicensed. In contrast, the majority TA cells appear to progress rapidly through the
465 cell-cycle, as many more actively incorporate EdU (**Figure 4A**).

466 We next confirmed that the unlicensed cells at the crypt base were Lgr5(+) stem cells. As it
467 is not possible to identify Lgr5 in these experiments, as it is extracted along with unbound
468 Mcm2, we instead identified Paneth cells by UEA staining and considered all UEA(-) cells in
469 the crypt base to stem cells (**Figure 4B**). >50% of the UEA(-) stem cells were in an unlicensed
470 state and were not incorporating EdU (**Figure 4C**). Approximately 30-40% of all UEA(-) cells
471 in the stem cell compartment were in an active phase of the cell cycle (licensed $G_1$, S or $G_2$;
472 **Figure 4C**), corresponding to 5-6 stem cells out of the total 14 present (Snippert et al.,
473 2010). This number is similar to the small number of proposed 'working' stem cells in the
474 crypt base (Baker et al., 2014, Kozar et al., 2013). Unlicensed cells not incorporating EdU (i.e.
475 unlabelled in this experiment) could theoretically be in either $G_0$ or in $G_2$. To distinguish
476 between these possibilities we first isolated crypt cells from Lgr5-GFP mice and measured
477 both GFP and DNA content. Both Lgr5(+) and Lgr5(-) cell populations had a similar cell-cycle
478 profile with the majority of cells having 2N DNA content (**S2 Figure C**). We also examined the
479 nuclear volume of cells at different positions along the crypt axis, after staining for EdU
480 incorporation and DNA-bound Mcm2. The majority of unlicensed cells had a similar nuclear
481 volume to that of fully licensed cells in $G_1$ and not cells in Late-S/$G_2$ phase (**S2 Figure D**).
482 Together, these results suggest that, although they express abundant Mcm2, the majority of
483 intestinal stem cells reside in an unlicensed $G_1$ state.

484 To confirm this conclusion, we flow-sorted unextracted Lgr5-GFP(+) cells, extracted
485 unbound MCM2-7 and stained them for Mcm2 and Ki67. Consistent with our previous
486 results, most Lgr5(+) cells with a 2N DNA content had low levels of DNA-bound Mcm2, and

487 were in an unlicensed state (**Figure 4Di, ii**). Importantly, both the licensed and unlicensed
488 cells were Ki67(+) indicating that they had not withdrawn from the cell-cycle long-term
489 (**Figure 4Dii**).

490 This unlicensed $G_1$ state - 2N DNA content, high Mcm2 expression but with low levels of
491 DNA-bound Mcm2 - could be explained by two, slightly different, scenarios. 1) MCM2-7 are
492 loaded on to DNA slowly in Lgr5(+) cells, thereby extending $G_1$ (Schepers et al., 2011)
493 (Dalton, 2015); or 2) Most Lgr5(+) cells enter $G_1$ and remain in an unlicensed state but do
494 not load MCM2-7 until an active decision is made to commit to cell cycle progression and
495 activate the licensing system, at which time MCM2-7 proteins are rapidly loaded. In option
496 1) where licensing is slow, the presence of unlicensed cells simply reflects the increased
497 time required to fully license origins, and different levels of Mcm2 loading should be equally
498 distributed between $G_1$ cells. In option 2), however, where there is an early stage of G1
499 where licensing does not occur, there should be a discrete peak of unlicensed cells with a $G_1$
500 DNA content representing cells that have withdrawn from the cell cycle, and a lower
501 frequency of $G_1$ cells that have loaded different amounts of MCM2-7. To distinguish
502 between these two possibilities, we utilized ergodic rate analysis. When examining the
503 frequency distribution of DNA-bound Mcm2 in Lgr5(+) cells with 2N DNA content we found
504 a discrete peak of unlicensed cells (**Figure 4E**) consistent with the second model. To confirm
505 these observations, we performed computer modelling in which the licensing rate was
506 varied in the presence or absence of an initial $G_1$ period when licensing did not occur.
507 (**Figure 4F**). With no unlicensed G1 period and low licensing rates (**Figure 4F**, left hand
508 panels), G1 cells were equally distributed across the different degrees of licensing. With
509 faster licensing rates and no unlicensed G1 period, a distinct peak of fully licensed G1 cells

510 appeared, similar to what has been observed in cell lines. Only when an unlicensed G1
511 period was introduced did a distinct peak of unlicensed G1 cells appear (**Figure 4F**, left hand
512 panels). Since most of these unlicensed Lgr5(+) cells express abundant Mcm2 (**Figure 1D**),
513 this suggests that their $G_1$ is characterised by a long unlicensed period. This may explain why
514 the cell-cycle length of intestinal stem cells is significantly longer than transit-amplifying
515 cells (Schepers et al., 2011).

516 To further confirm that many intestinal stem cells exist in an unlicensed $G_1$ state, we
517 examined the expression of Fluorescence ubiquitination cell-cycle indicator (FUCCI)
518 reporters as an independent indicator of cell-cycle progression. We harvested intestinal
519 tissue from Fucci2aR mice (Mort et al., 2014), and examined the expression of the $G_1$
520 specific hCdt1(30/120) and $S/G_2/M$ specific hGeminin(1/110) reporters (**S4 Figure A**). As
521 expected, many TA cells were hGeminin(1/110)(+). We also noticed that terminally
522 differentiated cells, such as Paneth cells in the stem cell compartment, and cells at the tips
523 of villi expressed high levels of hCdt1(30/120) (**S4 Figure B**) reflecting accumulation of the
524 reporter in differentiated cells (Mort et al., 2014). However, we found that most Mcm2(+)
525 stem cells in the crypt base expressed very low levels of the hCdt1(30/120) reporter, and
526 only few cells expressed high levels (**S4 Figure C, D**). In contrast, the majority of TA cells
527 were either hGeminin(1/110)$^{High}$ or hCdt1(30/120)$^{low}$, consistent with a short $G_1$ phase.
528 Together, this suggests that stem cells remain in a paused unlicensed $G_1$ state where they
529 do not rapidly accumulate hCdt1(30/120) unlike rapidly proliferating cells.

530 It has previously been reported that embryonic stem cells license more replication origins
531 than neural stem/progenitor cells differentiated from them (Ge et al., 2015). To determine if
532 adult stem and non-stem cells in intestinal crypts exhibit such differences, we compared the

533 amount of DNA-bound Mcm2 in $G_1/G_0$ and early S phase Lgr5(+) cells with that in Lgr5(-)
534 cells (Moreno et al., 2016). Although the majority of Lgr5(+) cells were unlicensed, when
535 they entered S phase they had approximately twice as much DNA-bound Mcm2 compared
536 to Lgr5(-) cells (**Figure 4G**). This is consistent with the idea that adult intestinal stem cells
537 license more origins than TA cells and may represent a mechanism to protect genomic
538 integrity.

539 **Intestinal label retaining cells are in a deep $G_0$ state**

540 Although the intestinal crypt base primarily consists of Lgr5(+) stem cells there is also a
541 reserved pool of quiescent stem cells, often referred to as '+4 label retaining cells' (LRCs)
542 reflecting their position in the crypt base and their ability to retain nascent DNA labels
543 (Potten et al., 2002). These cells are a rare subset of Lgr5(+) cells and are also secretory
544 precursors (Buczacki et al., 2013). To further define the licensing status of these label-
545 retaining intestinal stem cells, we identified UEA(-) LRCs by expressing H2B-GFP (which is
546 incorporated into the chromatin of dividing cells) for 7 days and then chasing for a further 7
547 days (Buczacki et al., 2013, Roth et al., 2012). Labelled cells that did not divide during the 7-
548 day chase period contain high levels of H2B-GFP (hence are LRCs), but cells that divided
549 multiple times only have low levels. LRCs were then distinguished from Paneth cells based
550 on UEA staining (**Figure 5A**). After induction, most cells in the epithelium expressed H2B-
551 GFP (**Figure 5Bi**). After the 7D chase, H2B-GFP expression was restricted to cells near the
552 villus tips, and cells at the crypt base (**Figure 5Bii**). We could successfully distinguish
553 between Paneth cells and LRCs on the basis of UEA staining (**Figure 5Bii**). Unlike the majority
554 of the Lgr5(+) cells, LRCs with high GFP-H2B did not express Mcm2 (**Figure 5C**). As expected,

555 only non-LRC daughter cells with low levels of H2B-GFP had DNA-bound Mcm2 (**Figure 5D**).
556 This shows that, LRC stem cells are in deep $G_0$, unable to license because they do not
557 express MCM2-7. In contrast, 'active' intestinal stem cells mostly reside in an unlicensed $G_1$
558 state.

559 **Licensing dynamics in intestinal organoids**

560 Intestinal stem cells reside in a highly specialised niche at the base of crypts. It is therefore
561 possible that this niche specifically allows stem cells to pause in an unlicensed $G_1$ state
562 where origin licensing is prevented until a further proliferative fate signal is received. To
563 understand the contribution of the stem cell niche to the dynamics of entry and exit from
564 the unlicensed $G_1$ state, we used intestinal organoids, which allowed us to manipulate the
565 stem cell niche/environment with small-molecules. Although the distribution of licensed
566 cells was similar between the branches of intestinal organoids and crypts in tissue, there
567 were considerably more cells with DNA-bound Mcm2 in the former (**Figure 6A, Ciii**).
568 Importantly, cells in organoids showed a discrete peak of fully licensed $G_1$ cells in addition to
569 the cells in the unlicensed $G_1$ state (**Figure 6Bii**). This suggests that the epithelium in
570 organoids represents an accelerated state of self-renewal and may not fully recapitulate
571 cell-cycle dynamics of intestinal epithelial cells *in vivo*.

572 We designed an assay to robustly assess licensing dynamics during entry and exit from the
573 unlicensed $G_1$ state, and transition towards $G_0$. Specifically, we used flow cytometry based
574 quantification of DNA-bound Mcm2, Ki67 and DNA content to measure licensing dynamics
575 during entry and exit from the unlicensed $G_1$ state, and transition towards $G_0$ (**S5 figure A**).
576 Most cells in organoids express Ki67 and it increased during cell-cycle progression (**Figure**

577 **6Bi**). The DNA-bound Mcm2 profile was similar to that in isolated crypts (**Figure 6Bii**).
578 Correlating Ki67 and DNA-bound Mcm2 produced a distinctive profile that is similar for
579 isolated cells from organoids (**Figure 6Ci**) and intestinal crypts (**Figure 6Cii**). This profile
580 reveals a population of cells that appear to lose Ki67 (dashed arrow in **Figure 6Cii**) and may
581 represent cells decreasing in proliferative capacity and transitioning towards differentiation
582 (**S5 Figure A**). Such a loss of proliferative capacity appeared to initiate in cells that express
583 Ki67 but are unlicensed, i.e. cells in unlicensed $G_1$. These data suggest that different stages
584 of quiescence can exist that reflected by a spectrum of Ki67 and Mcm levels.

585 Stem-cell niche maintenance in organoids mainly depends on a combination of EGF, Wnt
586 and Notch signalling (Sato et al., 2011). To identify the pathway that can modulate the
587 unlicensed $G_1$ state, we systematically treated organoids with a small molecule inhibitor of
588 EGFR (Gefitinib), a Wnt agonist (Chir99021), and a Notch activator (Valproic acid). Short-
589 term treatment with Gefitinib, which reduces MAP kinase activity and blocks DNA
590 replication and cell division (Lynch et al., 2004), immediately caused cells to accumulate in
591 the unlicensed $G_1$ state, with a 2N DNA content but continuing to express Mcm2 and Ki67
592 (**Figure 6D, E**). Only prolonged EGFR inhibition (4 days) caused transition to an intermediate
593 $G_0$ state, with significantly reduced Ki67 expression but with total Mcm2 levels maintained
594 (**Figure 6D, E**). Both states were reversed by removal of EGFRi and addition of fresh growth
595 factors (**Figure 6D, E**). Previously it was shown that EGFR increases Lgr5 expression (Basak et
596 al., 2017), suggesting that these transitional states (Unlicensed $G_1$ and $G_0$) are associated
597 with 'stemness'. Additionally, EGFRi appeared to potently kill transit-amplifying cells (**S5**
598 **Figure B, C**), leaving branches containing only stem cells (Basak et al., 2017). This suggests

599 that both, the fully quiescent $G_0$ and unlicensed $G_1$ states, may provide protection to stem
600 cells.

601 Treatment with the Wnt agonist Chir99021 did not appear to significantly affect licensing
602 dynamics (**S5 Figure C**). Strikingly, treatment with the Valproic acid (a Notch activator) alone
603 or in combination with Chir99021 significantly altered licensing profiles (**S5 Figure D, F**). The
604 combination of Chir99021 and Valproic acid induces Lgr5 expression throughout the
605 organoid epithelium (**S5 Figure E**) (Yin et al., 2014). Our data showed that this is associated
606 with the appearance of a population of cells with low levels of Ki67 and intermediate levels
607 of DNA-bound Mcm2 (**S5 Figure D**) similar to the intermediate, shallow $G_0$ state induced by
608 EGFRi. Surprisingly, we observed an arc of cells connecting this to the fully licensed state,
609 suggesting that re-licensing of these cells occurs before they express high levels of Ki67 and
610 that cells can reactivate licensing from a deeper state of $G_0$ directly (**S5 Figure D, F**).

611 Inhibiting Notch signalling with DAPT, which induces terminal secretory cell differentiation
612 (van Es et al., 2005), also significantly altered licensing dynamics and induced deep $G_0$, with
613 reduced Ki67 and loss of Mcm2 proteins (**S5 Figure G**). Together, these data suggest that
614 both EGFR signalling and Notch signalling can significantly influence the licensing dynamics
615 during the transition between quiescence and unlicensed $G_1$.

616 **The Unlicensed-$G_1$ state is lost in *Apc* mutant organoids**

617 Many established cell lines appear to lack an unlicensed $G_1$ state, instead licensing all origins
618 immediately upon mitotic exit (Friedrich et al., 2005, Haland et al., 2015, Moreno et al.,
619 2016, Matson et al., 2017). In addition, many of these cell-lines lack a functional licensing
620 checkpoint (Shreeram et al., 2002, Feng et al., 2003, Liu et al., 2009, Nevis et al., 2009) that

621 has been suggested to arrest cells in $G_1$ by inactivation of the RB-E2F restriction point(Liu et
622 al., 2009, Machida et al., 2005, Nevis et al., 2009, Shreeram et al., 2002, Teer et al., 2006).
623 To understand the biological relevance of the unlicensed $G_1$ state, we determined whether
624 origin licensing dynamics during $G_1$ are altered during the initial stages of tumorigenesis.

625 The first initiating mutations in colorectal cancer are usually in *Adenomatus polyposis coli*
626 *(*Apc). Therefore, we investigated whether licensing dynamics are altered in *Apc* mutant
627 intestinal epithelium. In $Apc^{Min/+}$ epithelium *in vivo*, Mcm2 expression appeared normal in
628 areas of normal histology but was greatly increased in polyps (**Figure 7A**). In isolated
629 $Apc^{Min/+}$ crypts, there was a slight increase in the size of the proliferative compartment
630 similar to previous reports (Trani et al., 2014), and a slight increase in the number of EdU(+)
631 cells in the stem cell compartment (**Figure 7Bi, iii**). However, in the majority of crypts there
632 were no significant differences in the number or distribution of licenced cells in the stem cell
633 compartment (**Figure 7Bi, iii**). However, we found a small number of crypts that were
634 considerably larger. Strikingly, within these crypts, we noticed small 'ribbons' of EdU(+) cells
635 that extended significantly into the transit-amplifying compartment (**Figure 7Bii**). We
636 suspected that these ribbons reflected a clone of cells that had undergone loss of
637 heterozygosity (LOH), and continually re-engage with the cell cycle. This in turn suggests
638 that the LOH event that converts $Apc^{Min/+}$ to $Apc^{Min/Min}$ cells significantly alters cell-cycle
639 dynamics.

640 To determine whether LOH alters origin licensing dynamics by modifying $G_1$, we compared
641 wild-type and $Apc^{Min/Min}$ organoids (**Figure 7C**). $Apc^{Min/Min}$ organoids contained many more
642 licensed cells that were distributed randomly throughout the organoid (**Figure 7D**),
643 reminiscent of the altered distribution of Ki67 (+) cells in these organoids (Fatehullah et al.,

644 2013). Strikingly, we found that licensing dynamics in the $G_1$ phase of *Apc*$^{Min/Min}$ cells were
645 significantly different and there was a significant loss of the unlicensed $G_1$ population.
646 (**Figure 7E**). Instead, there was a significant population of cells that appear to license
647 immediately upon $G_1$ entry and progressed into S-phase immediately after minimal licensing
648 (**Figure 7E, F**). Interestingly, we still detected a population of cells that licensed as many
649 origins as in WT organoids. These may be *Apc*$^{Min/+}$ cells that had not undergone LOH yet and
650 thus maintained near-normal cell cycle dynamics.

651 A functional licensing checkpoint depends on an intact RB restriction point and we tested
652 whether there the relative amounts of hypo- and hyper-phosphorylated RB varied between
653 wild type and *Apc*$^{Min/Min}$ epithelia. In *wild-type* organoids, we noticed that the majority of RB
654 appeared hypo-phosphorylated (**Figure 7G**). In contrast, in *Apc*$^{Min/Min}$ organoids, at least half
655 of RB appeared hyper-phosphorylated, with at least 3-fold more phosphorylated RB.
656 Together, this data is consistent with the idea that cells exist in an unlicensed $G_1$ state prior
657 to passage through the restriction point and activation of E2F-driven transcription. In
658 contrast, *Apc* mutant cells appear to have lost normal restriction point control, so that they
659 have constitutively hyper-phosphorylated RB, allowing them to completely bypass the
660 unlicensed $G_1$ state.

661

662 **Discussion**

663 The cell-cycle of intestinal stem and transit-amplifying cells is poorly understood. By
664 comparing the total and DNA-bound Mcm2 in intact intestinal crypts we provide new
665 insights into how licensing and cell-cycle commitment are coupled in this tissue. We provide

666 evidence that after their final mitosis, transit amplifying cells do not license their replication
667 origins and immediately exit the cell cycle. We show that many Lgr5(+) stem cells spend the
668 majority of $G_1$ in an unlicensed state, continually expressing Mcm2 and Ki67. In unlicensed-
669 $G_1$, stem cells could be poised to respond to cues and progress past this restriction point to
670 resume the cell division cycle.

671 Lgr5(+) stem cells have a cell-cycle length greater than transit-amplifying cells (Schepers et
672 al., 2011). The biological relevance of this is currently unknown. The data presented here
673 suggest a delay in origin licensing is a key feature of the prolonged cell-cycle of Lgr5(+) cells.
674 Although ~80% of Lgr5(+) cells are thought to be continually proliferative and express high
675 levels of both Ki67 (Basak et al., 2014) and Mcm2, we found that most Lgr5(+) cells reside in
676 an unlicensed state, with 2N DNA content and Mcm2 not bound to DNA. Since the licensed
677 state defines proliferative fate commitment (Blow and Hodgson, 2002), we suggest that
678 these cells are temporarily paused in $G_1$, continuing to express proliferative makers such as
679 Ki67 and Mcm2, but without fully committing to the cell cycle (**Figure 8**). We show that the
680 number of Lgr5(+) cells with DNA bound-Mcm2 was similar to the number of proposed
681 'active' stem cells determined in lineage tracing experiments (Baker et al., 2014, Kozar et al.,
682 2013).

683 Prolonged arrest may eventually result in degradation of MCM2-7 proteins and lead to
684 induction of a state of deep quiescence ($G_0$). Consistent with this idea, we observed that
685 LRCs, thought to provide a reserve of quiescent stem cells, did not express Mcm2. The lack
686 of Mcm2 expression may reflect that a significant period of time has passed since these cells
687 divided. The delay in activating the licensing system may create a prolonged time-window
688 for Lgr5(+) cells to receive and interpret environmental cues before deciding to commit to

689 duplication, offering a means to control their number. It is likely that the majority of Lgr5(+)
690 cells regularly resume their cell cycle, given their continual expression of proliferation
691 markers (Basak et al., 2014). The identity and decisions of Lgr5(+) cells are governed by
692 stochastic choices and the ability to pause briefly in $G_1$ offers them unique flexibility in
693 making these choices.

694 As expected, the transition from unlicensed $G_1$ to licensed $G_1$ seems dependent on EGFR
695 signalling. However, other pathways responsible for stem-cell maintenance can also
696 significantly cause the appearance of a unique population of unlicensed cells with distinct
697 cell-cycle dynamics. Growing evidence suggests that intestinal stem cell fate is not governed
698 by asymmetric segregation of fate determinants (Lopez-Garcia et al., 2010, Snippert et al.,
699 2010, Steinhauser et al., 2012). Instead, factors operating in the stem cell niche, such as Wnt
700 and Notch signalling affect stem cell fate decisions and also reduce the cycle rate of
701 intestinal stem cells (Hirata et al., 2013). This is consistent with the idea that cell fate
702 choices are affected by decreasing proliferation rate and increased $G_0/G_1$ length. Indeed,
703 extending $G_1$ in mouse and human embryonic stem cells can drive differentiation (Calder et
704 al., 2013, Coronado et al., 2013). Similarly, long $G_1$ phases are associated with the
705 generation of fate-restricted progenitors during neurogenesis (Arai et al., 2011). An
706 extended time window in the cell-cycle has been suggested to allow niche factors and/or
707 fate determinants to accumulate to direct progenitor fate (Calegari and Huttner, 2003). In
708 the case of adult intestinal stem cells, holding cells in $G_1$ may allow an extended time for
709 stem cell fate factors to act and maintain stem cell fate. In contrast, many embryonic stem
710 cells licence rapidly and the cell cycle slows throughout differentiation (Matson et al., 2017).

711 However, like embryonic stem cells (Ge et al., 2015), intestinal stem cells appear to have
712 licensed more origins than non-stem cells when they enter S phase. This may help ensure
713 accurate and complete genome duplication in long-lived stem cells (Moreno et al., 2016).
714 With a higher demand for licensed origins, intestinal stem cells may therefore more readily
715 engage the licensing checkpoint that ensures that all origins are licensed before cells enter S
716 phase (Alver et al., 2014, Liu et al., 2009, Shreeram et al., 2002). This additional demand for
717 licensed origins in stem cells may also explain why crypts hypomorphic for Mcm2 have a
718 stem-cell deficiency (Pruitt et al., 2007).

719 It is unclear how intestinal stem cells enter a significant unlicensed $G_1$ state. The simplest
720 explanation is that licensing factors such as Cdt1 or Cdc6 are not readily available in new-
721 born stem cells, and their synthesis has to be stimulated by an upstream signal for fate
722 commitment via activation of E2F-driven transcription. This is the situation after prolonged
723 quiescence, which is accompanied by passive downregulation of licensing factors (Coller,
724 2007). In contrast, in continually dividing cells their levels are maintained. Consistent with
725 this idea, licensing factors such as Cdc6, along with many cyclin-CDK complexes, are down
726 regulated beyond the end of the TA zone (Frey et al., 2000) (Smartt et al., 2007). Cells
727 without a functional restriction point, such as *Apc* mutant cells or most cancer cell lines,
728 could immediately license their origins upon entering $G_1$ and can progress into S-phase
729 without sufficient origins being licensed. Interestingly, both transit-amplifying cells and
730 highly proliferative *Apc* mutant cells are highly sensitive to replication inhibitors, such as
731 Gefitinib (**S5 Figure H**). Wild-type stem cells survive this treatment, potentially by engaging
732 the licensing checkpoint to reversibly stall in Unlicensed $G_1$. This suggests that the
733 unlicensed $G_1$ can protect stem cells from replication inhibitors and offers a potentially

734 selective means to kill highly proliferative cells, such as *Apc* mutant cells (Shreeram et al.,
735 2002, Blow and Gillespie, 2008).

736 In summary, we demonstrate that the dynamics of the DNA replication licensing system
737 provides a new way for measuring the proliferative fate of intestinal stem cells. We suggest
738 a model for 'working' intestinal stem cells that spend a significant proportion of $G_1$ in a
739 unlicensed state until a proliferative fate decision is made. Correspondingly, exit from the
740 cell-cycle in label retaining '+4' cells leads to loss of proliferative capacity and loss of Mcm2
741 expression causing cells to enter a deeply $G_0$ quiescent state (**Figure 6**). The unlicensed $G_1$
742 state is lost in *Apc* mutant epithelia, which lack a functional Rb-restriction point. We suggest
743 that the unlicensed $G_1$ state serves stem cells in controlling their numbers by regulating the
744 cell-cycle.

745 **Author contributions**

746 T.D.C, J.J.B and I.N conceived and designed the study; T.D.C and I.P.N collected the data; Y.C
747 assisted with organoid experiments; T.D.C performed the data analysis. J.J.B performed the
748 modelling simulations. T.D.C, I.N and J.J.B wrote the manuscript.

749 **Conflicts of Interest**

750 The authors report no conflicts of interest.

751 **Acknowledgements**

752 We would like to thank members of the Näthke and Blow laboratories for general assistance
753 and helpful discussions; Dr Paul Appleton, Dr Graeme Ball and the Dundee Imaging and
754 Tissue Imaging Facility for support with microscopy and image analysis. The imaging facility

755 is funded by the Welcome Trust Technology Platform award (097945/B/11/Z) and Welcome
756 Trust award (101468/Z/13/Z). We thank Dr Rosemary Clarke and the Dundee Flow
757 Cytometry Facility for support with flow cytometry, cell sorting and analysis. We also thank
758 Dr Richard Mort (University of Edinburgh) for Fucci2aR mouse tissue. This work was
759 supported by a programme grant from Cancer Research UK to I.N (C430/A11243) and to
760 J.J.B (C303/A14301), Wellcome Trust grant WT096598MA and an MRC studentship award to
761 T.D.C.

762

763 **REFERENCES**

764 ALVER, R. C., CHADHA, G. S. & BLOW, J. J. 2014. The contribution of dormant origins to
765 genome stability: from cell biology to human genetics. *DNA repair,* 19**,** 182-9.
766 ARAI, Y., PULVERS, J. N., HAFFNER, C., SCHILLING, B., NUSSLEIN, I., CALEGARI, F. & HUTTNER,
767 W. B. 2011. Neural stem and progenitor cells shorten S-phase on commitment to
768 neuron production. *Nature communications,* 2**,** 154.
769 BAKER, A. M., CERESER, B., MELTON, S., FLETCHER, A. G., RODRIGUEZ-JUSTO, M., TADROUS,
770 P. J., HUMPHRIES, A., ELIA, G., MCDONALD, S. A., WRIGHT, N. A., SIMONS, B. D.,
771 JANSEN, M. & GRAHAM, T. A. 2014. Quantification of crypt and stem cell evolution in
772 the normal and neoplastic human colon. *Cell reports,* 8**,** 940-7.
773 BARKER, N., VAN ES, J. H., KUIPERS, J., KUJALA, P., VAN DEN BORN, M., COZIJNSEN, M.,
774 HAEGEBARTH, A., KORVING, J., BEGTHEL, H., PETERS, P. J. & CLEVERS, H. 2007.
775 Identification of stem cells in small intestine and colon by marker gene Lgr5. *Nature,*
776 449**,** 1003-7.
777 BASAK, O., BEUMER, J., WIEBRANDS, K., SENO, H., VAN OUDENAARDEN, A. & CLEVERS, H.
778 2017. Induced Quiescence of Lgr5+ Stem Cells in Intestinal Organoids Enables
779 Differentiation of Hormone-Producing Enteroendocrine Cells. *Cell stem cell,* 20**,** 177-
780 190 e4.
781 BASAK, O., VAN DE BORN, M., KORVING, J., BEUMER, J., VAN DER ELST, S., VAN ES, J. H. &
782 CLEVERS, H. 2014. Mapping early fate determination in Lgr5+ crypt stem cells using a
783 novel Ki67-RFP allele. *The EMBO journal,* 33**,** 2057-68.
784 BLOW, J. J. & GILLESPIE, P. J. 2008. Replication licensing and cancer--a fatal entanglement?
785 *Nature reviews. Cancer,* 8**,** 799-806.
786 BLOW, J. J. & HODGSON, B. 2002. Replication licensing--defining the proliferative state?
787 *Trends in cell biology,* 12**,** 72-8.

788 BUCZACKI, S. J., ZECCHINI, H. I., NICHOLSON, A. M., RUSSELL, R., VERMEULEN, L., KEMP, R. &
789 WINTON, D. J. 2013. Intestinal label-retaining cells are secretory precursors
790 expressing Lgr5. *Nature,* 495**,** 65-9.
791 CALDER, A., ROTH-ALBIN, I., BHATIA, S., PILQUIL, C., LEE, J. H., BHATIA, M., LEVADOUX-
792 MARTIN, M., MCNICOL, J., RUSSELL, J., COLLINS, T. & DRAPER, J. S. 2013. Lengthened
793 G1 phase indicates differentiation status in human embryonic stem cells. *Stem cells*
794 *and development,* 22**,** 279-95.
795 CALEGARI, F. & HUTTNER, W. B. 2003. An inhibition of cyclin-dependent kinases that
796 lengthens, but does not arrest, neuroepithelial cell cycle induces premature
797 neurogenesis. *Journal of cell science,* 116**,** 4947-55.
798 CHAMPERIS TSANIRAS, S., KANELLAKIS, N., SYMEONIDOU, I. E., NIKOLOPOULOU, P.,
799 LYGEROU, Z. & TARAVIRAS, S. 2014. Licensing of DNA replication, cancer,
800 pluripotency and differentiation: an interlinked world? *Seminars in cell &*
801 *developmental biology,* 30**,** 174-80.
802 CHWALINSKI, S. & POTTEN, C. S. 1987. Influence of irradiation or thymidine (TdR) on the
803 pattern of 3H-TdR incorporation at each cell position in the crypts of the small
804 intestine of the mouse. *International journal of radiation biology and related studies*
805 *in physics, chemistry, and medicine,* 51**,** 243-54.
806 COLLER, H. A. 2007. What's taking so long? S-phase entry from quiescence versus
807 proliferation. *Nature reviews. Molecular cell biology,* 8**,** 667-70.
808 CORONADO, D., GODET, M., BOURILLOT, P. Y., TAPPONNIER, Y., BERNAT, A., PETIT, M.,
809 AFANASSIEFF, M., MARKOSSIAN, S., MALASHICHEVA, A., IACONE, R., ANASTASSIADIS,
810 K. & SAVATIER, P. 2013. A short G1 phase is an intrinsic determinant of naive
811 embryonic stem cell pluripotency. *Stem cell research,* 10**,** 118-31.
812 DALTON, S. 2015. Linking the Cell Cycle to Cell Fate Decisions. *Trends in cell biology,* 25**,** 592-
813 600.
814 DIMITROVA, D. S., PROKHOROVA, T. A., BLOW, J. J., TODOROV, I. T. & GILBERT, D. M. 2002.
815 Mammalian nuclei become licensed for DNA replication during late telophase.
816 *Journal of cell science,* 115**,** 51-9.
817 EVRIN, C., CLARKE, P., ZECH, J., LURZ, R., SUN, J., UHLE, S., LI, H., STILLMAN, B. & SPECK, C.
818 2009. A double-hexameric MCM2-7 complex is loaded onto origin DNA during
819 licensing of eukaryotic DNA replication. *Proceedings of the National Academy of*
820 *Sciences of the United States of America,* 106**,** 20240-5.
821 EWARD, K. L., OBERMANN, E. C., SHREERAM, S., LODDO, M., FANSHAWE, T., WILLIAMS, C.,
822 JUNG, H. I., PREVOST, A. T., BLOW, J. J., STOEBER, K. & WILLIAMS, G. H. 2004. DNA
823 replication licensing in somatic and germ cells. *Journal of cell science,* 117**,** 5875-86.
824 FATEHULLAH, A., APPLETON, P. L. & NATHKE, I. S. 2013. Cell and tissue polarity in the
825 intestinal tract during tumourigenesis: cells still know the right way up, but tissue
826 organization is lost. *Philosophical transactions of the Royal Society of London. Series*
827 *B, Biological sciences,* 368**,** 20130014.
828 FENG, D., TU, Z., WU, W. & LIANG, C. 2003. Inhibiting the expression of DNA replication-
829 initiation proteins induces apoptosis in human cancer cells. *Cancer research,* 63**,**
830 7356-64.
831 FREY, M. R., CLARK, J. A., LEONTIEVA, O., URONIS, J. M., BLACK, A. R. & BLACK, J. D. 2000.
832 Protein kinase C signaling mediates a program of cell cycle withdrawal in the
833 intestinal epithelium. *The Journal of cell biology,* 151**,** 763-78.

834 FRIEDRICH, T. D., BEDNER, E., DARZYNKIEWICZ, Z. & LEHMAN, J. M. 2005. Distinct patterns
835 of MCM protein binding in nuclei of S phase and rereplicating SV40-infected monkey
836 kidney cells. *Cytometry. Part A : the journal of the International Society for Analytical*
837 *Cytology,* 68**,** 10-8.
838 GAMBUS, A., KHOUDOLI, G. A., JONES, R. C. & BLOW, J. J. 2011. MCM2-7 form double
839 hexamers at licensed origins in Xenopus egg extract. *The Journal of biological*
840 *chemistry,* 286**,** 11855-64.
841 GE, X. Q., HAN, J., CHENG, E. C., YAMAGUCHI, S., SHIMA, N., THOMAS, J. L. & LIN, H. 2015.
842 Embryonic Stem Cells License a High Level of Dormant Origins to Protect the
843 Genome against Replication Stress. *Stem cell reports,* 5**,** 185-94.
844 GONZALEZ, M. A., TACHIBANA, K. E., LASKEY, R. A. & COLEMAN, N. 2005. Control of DNA
845 replication and its potential clinical exploitation. *Nature reviews. Cancer,* 5**,** 135-41.
846 HALAND, T. W., BOYE, E., STOKKE, T., GRALLERT, B. & SYLJUASEN, R. G. 2015. Simultaneous
847 measurement of passage through the restriction point and MCM loading in single
848 cells. *Nucleic acids research,* 43**,** e150.
849 HIRATA, A., UTIKAL, J., YAMASHITA, S., AOKI, H., WATANABE, A., YAMAMOTO, T., OKANO,
850 H., BARDEESY, N., KUNISADA, T., USHIJIMA, T., HARA, A., JAENISCH, R.,
851 HOCHEDLINGER, K. & YAMADA, Y. 2013. Dose-dependent roles for canonical Wnt
852 signalling in de novo crypt formation and cell cycle properties of the colonic
853 epithelium. *Development,* 140**,** 66-75.
854 ILVES, I., PETOJEVIC, T., PESAVENTO, J. J. & BOTCHAN, M. R. 2010. Activation of the MCM2-7
855 helicase by association with Cdc45 and GINS proteins. *Molecular cell,* 37**,** 247-58.
856 JURIKOVA, M., DANIHEL, L., POLAK, S. & VARGA, I. 2016. Ki67, PCNA, and MCM proteins:
857 Markers of proliferation in the diagnosis of breast cancer. *Acta histochemica,* 118**,**
858 544-52.
859 KINGSBURY, S. R., LODDO, M., FANSHAWE, T., OBERMANN, E. C., PREVOST, A. T., STOEBER,
860 K. & WILLIAMS, G. H. 2005. Repression of DNA replication licensing in quiescence is
861 independent of geminin and may define the cell cycle state of progenitor cells.
862 *Experimental cell research,* 309**,** 56-67.
863 KOZAR, S., MORRISSEY, E., NICHOLSON, A. M., VAN DER HEIJDEN, M., ZECCHINI, H. I., KEMP,
864 R., TAVARE, S., VERMEULEN, L. & WINTON, D. J. 2013. Continuous clonal labeling
865 reveals small numbers of functional stem cells in intestinal crypts and adenomas. *Cell*
866 *stem cell,* 13**,** 626-33.
867 KRUDE, T., MUSAHL, C., LASKEY, R. A. & KNIPPERS, R. 1996. Human replication proteins
868 hCdc21, hCdc46 and P1Mcm3 bind chromatin uniformly before S-phase and are
869 displaced locally during DNA replication. *Journal of cell science,* 109 ( Pt 2)**,** 309-18.
870 LEONE, G., DEGREGORI, J., YAN, Z., JAKOI, L., ISHIDA, S., WILLIAMS, R. S. & NEVINS, J. R.
871 1998. E2F3 activity is regulated during the cell cycle and is required for the induction
872 of S phase. *Genes & development,* 12**,** 2120-30.
873 LIU, P., SLATER, D. M., LENBURG, M., NEVIS, K., COOK, J. G. & VAZIRI, C. 2009. Replication
874 licensing promotes cyclin D1 expression and G1 progression in untransformed
875 human cells. *Cell cycle,* 8**,** 125-36.
876 LOPEZ-GARCIA, C., KLEIN, A. M., SIMONS, B. D. & WINTON, D. J. 2010. Intestinal stem cell
877 replacement follows a pattern of neutral drift. *Science,* 330**,** 822-5.
878 LYNCH, T. J., BELL, D. W., SORDELLA, R., GURUBHAGAVATULA, S., OKIMOTO, R. A.,
879 BRANNIGAN, B. W., HARRIS, P. L., HASERLAT, S. M., SUPKO, J. G., HALUSKA, F. G.,

880 LOUIS, D. N., CHRISTIANI, D. C., SETTLEMAN, J. & HABER, D. A. 2004. Activating
881 mutations in the epidermal growth factor receptor underlying responsiveness of
882 non-small-cell lung cancer to gefitinib. *The New England journal of medicine,* 350**,**
883 2129-39.
884 MACHIDA, Y. J., TEER, J. K. & DUTTA, A. 2005. Acute reduction of an origin recognition
885 complex (ORC) subunit in human cells reveals a requirement of ORC for Cdk2
886 activation. *The Journal of biological chemistry,* 280**,** 27624-30.
887 MAKAROVA, K. S., KOONIN, E. V. & KELMAN, Z. 2012. The CMG (CDC45/RecJ, MCM, GINS)
888 complex is a conserved component of the DNA replication system in all archaea and
889 eukaryotes. *Biology direct,* 7**,** 7.
890 MATSON, J. P., DUMITRU, R., CORYELL, P., BAXLEY, R. M., CHEN, W., TWAROSKI, K.,
891 WEBBER, B. R., TOLAR, J., BIELINSKY, A. K., PURVIS, J. E. & COOK, J. G. 2017. Rapid
892 DNA replication origin licensing protects stem cell pluripotency. *eLife,* 6.
893 MORENO, A., CARRINGTON, J. T., ALBERGANTE, L., AL MAMUN, M., HAAGENSEN, E. J.,
894 KOMSELI, E. S., GORGOULIS, V. G., NEWMAN, T. J. & BLOW, J. J. 2016. Unreplicated
895 DNA remaining from unperturbed S phases passes through mitosis for resolution in
896 daughter cells. *Proceedings of the National Academy of Sciences of the United States*
897 *of America,* 113**,** E5757-64.
898 MORT, R. L., FORD, M. J., SAKAUE-SAWANO, A., LINDSTROM, N. O., CASADIO, A., DOUGLAS,
899 A. T., KEIGHREN, M. A., HOHENSTEIN, P., MIYAWAKI, A. & JACKSON, I. J. 2014.
900 Fucci2a: a bicistronic cell cycle reporter that allows Cre mediated tissue specific
901 expression in mice. *Cell cycle,* 13**,** 2681-96.
902 MOYER, S. E., LEWIS, P. W. & BOTCHAN, M. R. 2006. Isolation of the Cdc45/Mcm2-7/GINS
903 (CMG) complex, a candidate for the eukaryotic DNA replication fork helicase.
904 *Proceedings of the National Academy of Sciences of the United States of America,*
905 103**,** 10236-41.
906 MUNOZ, J., STANGE, D. E., SCHEPERS, A. G., VAN DE WETERING, M., KOO, B. K., ITZKOVITZ,
907 S., VOLCKMANN, R., KUNG, K. S., KOSTER, J., RADULESCU, S., MYANT, K., VERSTEEG,
908 R., SANSOM, O. J., VAN ES, J. H., BARKER, N., VAN OUDENAARDEN, A., MOHAMMED,
909 S., HECK, A. J. & CLEVERS, H. 2012. The Lgr5 intestinal stem cell signature: robust
910 expression of proposed quiescent '+4' cell markers. *The EMBO journal,* 31**,** 3079-91.
911 MUSAHL, C., HOLTHOFF, H. P., LESCH, R. & KNIPPERS, R. 1998. Stability of the replicative
912 Mcm3 protein in proliferating and differentiating human cells. *Experimental cell*
913 *research,* 241**,** 260-4.
914 NAMDAR, M. & KEARSEY, S. E. 2006. Analysis of Mcm2-7 chromatin binding during anaphase
915 and in the transition to quiescence in fission yeast. *Experimental cell research,* 312**,**
916 3360-9.
917 NEVIS, K. R., CORDEIRO-STONE, M. & COOK, J. G. 2009. Origin licensing and p53 status
918 regulate Cdk2 activity during G(1). *Cell cycle,* 8**,** 1952-63.
919 OHTANI, K., IWANAGA, R., NAKAMURA, M., IKEDA, M., YABUTA, N., TSURUGA, H. & NOJIMA,
920 H. 1999. Cell growth-regulated expression of mammalian MCM5 and MCM6 genes
921 mediated by the transcription factor E2F. *Oncogene,* 18**,** 2299-309.
922 POTTEN, C. S. & LOEFFLER, M. 1990. Stem cells: attributes, cycles, spirals, pitfalls and
923 uncertainties. Lessons for and from the crypt. *Development,* 110**,** 1001-20.
924 POTTEN, C. S., OWEN, G. & BOOTH, D. 2002. Intestinal stem cells protect their genome by
925 selective segregation of template DNA strands. *Journal of cell science,* 115**,** 2381-8.

926 PRUITT, S. C., BAILEY, K. J. & FREELAND, A. 2007. Reduced Mcm2 expression results in severe
927 stem/progenitor cell deficiency and cancer. *Stem cells,* 25**,** 3121-32.
928 PRUITT, S. C., FREELAND, A. & KUDLA, A. 2010. Cell cycle heterogeneity in the small
929 intestinal crypt and maintenance of genome integrity. *Stem cells,* 28**,** 1250-9.
930 REMUS, D., BEURON, F., TOLUN, G., GRIFFITH, J. D., MORRIS, E. P. & DIFFLEY, J. F. 2009.
931 Concerted loading of Mcm2-7 double hexamers around DNA during DNA replication
932 origin licensing. *Cell,* 139**,** 719-30.
933 RHIND, N. & GILBERT, D. M. 2013. DNA replication timing. *Cold Spring Harbor perspectives in*
934 *biology,* 5**,** a010132.
935 ROTH, S., FRANKEN, P., SACCHETTI, A., KREMER, A., ANDERSON, K., SANSOM, O. & FODDE,
936 R. 2012. Paneth cells in intestinal homeostasis and tissue injury. *Plos One,* 7**,** e38965.
937 SATO, T., VAN ES, J. H., SNIPPERT, H. J., STANGE, D. E., VRIES, R. G., VAN DEN BORN, M.,
938 BARKER, N., SHROYER, N. F., VAN DE WETERING, M. & CLEVERS, H. 2011. Paneth cells
939 constitute the niche for Lgr5 stem cells in intestinal crypts. *Nature,* 469**,** 415-8.
940 SCHEPERS, A. G., VRIES, R., VAN DEN BORN, M., VAN DE WETERING, M. & CLEVERS, H. 2011.
941 Lgr5 intestinal stem cells have high telomerase activity and randomly segregate their
942 chromosomes. *The EMBO journal,* 30**,** 1104-9.
943 SHREERAM, S., SPARKS, A., LANE, D. P. & BLOW, J. J. 2002. Cell type-specific responses of
944 human cells to inhibition of replication licensing. *Oncogene,* 21**,** 6624-32.
945 SMARTT, H. J., GUILMEAU, S., NASSER, S. V., NICHOLAS, C., BANCROFT, L., SIMPSON, S. A.,
946 YEH, N., YANG, W., MARIADASON, J. M., KOFF, A. & AUGENLICHT, L. H. 2007. p27kip1
947 Regulates cdk2 activity in the proliferating zone of the mouse intestinal epithelium:
948 potential role in neoplasia. *Gastroenterology,* 133**,** 232-43.
949 SNIPPERT, H. J., VAN DER FLIER, L. G., SATO, T., VAN ES, J. H., VAN DEN BORN, M., KROON-
950 VEENBOER, C., BARKER, N., KLEIN, A. M., VAN RHEENEN, J., SIMONS, B. D. &
951 CLEVERS, H. 2010. Intestinal crypt homeostasis results from neutral competition
952 between symmetrically dividing Lgr5 stem cells. *Cell,* 143**,** 134-44.
953 STEINHAUSER, M. L., BAILEY, A. P., SENYO, S. E., GUILLERMIER, C., PERLSTEIN, T. S., GOULD,
954 A. P., LEE, R. T. & LECHENE, C. P. 2012. Multi-isotope imaging mass spectrometry
955 quantifies stem cell division and metabolism. *Nature,* 481**,** 516-9.
956 STOEBER, K., TLSTY, T. D., HAPPERFIELD, L., THOMAS, G. A., ROMANOV, S., BOBROW, L.,
957 WILLIAMS, E. D. & WILLIAMS, G. H. 2001. DNA replication licensing and human cell
958 proliferation. *Journal of cell science,* 114**,** 2027-41.
959 SYMEONIDOU, I. E., KOTSANTIS, P., ROUKOS, V., RAPSOMANIKI, M. A., GRECCO, H. E.,
960 BASTIAENS, P., TARAVIRAS, S. & LYGEROU, Z. 2013. Multi-step loading of human
961 minichromosome maintenance proteins in live human cells. *The Journal of biological*
962 *chemistry,* 288**,** 35852-67.
963 TEER, J. K., MACHIDA, Y. J., LABIT, H., NOVAC, O., HYRIEN, O., MARHEINEKE, K., ZANNIS-
964 HADJOPOULOS, M. & DUTTA, A. 2006. Proliferating human cells hypomorphic for
965 origin recognition complex 2 and pre-replicative complex formation have a defect in
966 p53 activation and Cdk2 kinase activation. *The Journal of biological chemistry,* 281**,**
967 6253-60.
968 TODOROV, I. T., WERNESS, B. A., WANG, H. Q., BUDDHARAJU, L. N., TODOROVA, P. D.,
969 SLOCUM, H. K., BROOKS, J. S. & HUBERMAN, J. A. 1998. HsMCM2/BM28: a novel
970 proliferation marker for human tumors and normal tissues. *Laboratory investigation;*
971 *a journal of technical methods and pathology,* 78**,** 73-8.

TRANI, D., NELSON, S. A., MOON, B. H., SWEDLOW, J. J., WILLIAMS, E. M., STRAWN, S. J., APPLETON, P. L., KALLAKURY, B., NATHKE, I. & FORNACE, A. J., JR. 2014. High-energy particle-induced tumorigenesis throughout the gastrointestinal tract. *Radiation research,* 181**,** 162-71.

VAN DER FLIER, L. G. & CLEVERS, H. 2009. Stem cells, self-renewal, and differentiation in the intestinal epithelium. *Annual review of physiology,* 71**,** 241-60.

VAN ES, J. H., VAN GIJN, M. E., RICCIO, O., VAN DEN BORN, M., VOOIJS, M., BEGTHEL, H., COZIJNSEN, M., ROBINE, S., WINTON, D. J., RADTKE, F. & CLEVERS, H. 2005. Notch/gamma-secretase inhibition turns proliferative cells in intestinal crypts and adenomas into goblet cells. *Nature,* 435**,** 959-63.

WILLIAMS, G. H., ROMANOWSKI, P., MORRIS, L., MADINE, M., MILLS, A. D., STOEBER, K., MARR, J., LASKEY, R. A. & COLEMAN, N. 1998. Improved cervical smear assessment using antibodies against proteins that regulate DNA replication. *Proceedings of the National Academy of Sciences of the United States of America,* 95**,** 14932-7.

WILLIAMS, G. H., SWINN, R., PREVOST, A. T., DE CLIVE-LOWE, P., HALSALL, I., GOING, J. J., HALES, C. N., STOEBER, K. & MIDDLETON, S. J. 2004. Diagnosis of oesophageal cancer by detection of minichromosome maintenance 5 protein in gastric aspirates. *British journal of cancer,* 91**,** 714-9.

YIN, X., FARIN, H. F., VAN ES, J. H., CLEVERS, H., LANGER, R. & KARP, J. M. 2014. Niche-independent high-purity cultures of Lgr5+ intestinal stem cells and their progeny. *Nature methods,* 11**,** 106-12.

995 **Figure Legends**

996 **Figure 1. Mcm2 is expressed ubiquitously along the crypt-villus axis and declines slowly as**
997 **cells differentiate**

998 (**A**) Sections of normal human (top panel) and mouse (bottom panel) small-intestine were
999 stained with Phalloidin (Green) and an antibody against Mcm2 (Red). Scale bars: 200 µm.

1000 (**B**) Mean Mcm2 intensities for segmented nuclei were plotted along the crypt-villus axis for
1001 mouse and human tissue. Location of the crypt and villus domains is indicated.

1002 (**C**) An intestinal crypt stained with Hoechst (Blue), Phalloidin (Green) and an antibody
1003 against Mcm2 (Red). Individual cells in interphase and mitosis (metaphase and cytokinesis)
1004 are outlined by dashed white lines.

1005 (**D**) Maximum intensity projections of whole-mount intestinal tissue revealing intestinal
1006 crypts and villi (left panels). Individual X-Y sections are also shown to reveal the epithelium
1007 (right panels). Tissue was stained with Phalloidin (Green) and Hoechst (Blue) and an
1008 antibody against Mcm2 (Red). The alternating pattern of Mcm2(+) (Green stars) and Mcm2(-
1009 ) (Orange stars) in the crypt base is highlighted)

1010 (**E**) Images of Lgr5-GFP stem cells (Green) (top panel) co-stained with a Mcm2 antibody
1011 (Red). The correlation (Pearson's correlation R=0.81, p<0.0001) between mean Mcm2 and
1012 Lgr5-GFP intensities for 69 Lgr5-GFP(+) cells normalised to the maximum intensity for an
1013 individual crypt is shown.

1014 (**F**) Images of UEA(+) Paneth Cells (top panels) co-stained with an Mcm2 antibody (Red) and
1015 UEA (Green). Mean Mcm2 intensity for segmented nuclei of UEA(+) Paneth cells was
1016 compared with interphase cells (Right panels).

1017 (**G**) Mcm2 (Green) and UEA (Red) expression in subsets of UEA(+) cells in crypt and villus
1018 domains. UEA(+) cells at the crypt base represent Paneth cells.

1019 (**H**) Quantification of mean Mcm2 intensity in individual UEA(+) cell populations. UEA(+) cells
1020 in the crypt base (Paneth cells, N=224), in the upper crypt compartment (Crypt, N = 132) and
1021 in the villus compartment (Villus, N = 225) were identified manually, and the nuclear Mcm2
1022 intensity was determined for individual cells (All cells, N = 33,736). There was a significant
1023 difference between UEA(+) cells in the crypt and villus compartments (T test, p<0.0001)

1024

1025 **Figure 2. Visualising Mcm2 licensing in intestinal crypts**

1026 (**A**) Representative bright-field images of extracted and unextracted isolated intestinal
1027 crypts. Scale bar: 90 µm

1028 (**B**) Representative images of isolated crypts stained with antibodies against Mcm2 (Red) or
1029 Ki67 (Purple). Scale bar: 10 µm

1030 (**C**) The Mcm2 labelling index for unextracted and extracted crypts is significantly different
1031 (Mean +/- SEM, N=10 crypts (T test, $p<0.0001$).

1032 (**D**) Representative intestinal crypts stained with Hoechst (Blue) and antibodies against
1033 Mcm2 (Red) and phospho-histone H3 (pH-H3) (Green).

1034 (**E**) Representative flow cytometry profiles for extracted and unextracted isolated crypt
1035 epithelial cells showing Mcm2 vs. DNA content.

1036 (**E'**) Suggested model of the licensing profile shown in panel E. Deeply quiescent cells, do not
1037 express Mcm2 and have a no detectable Mcm2 signal. Cells expressing soluble Mcm2
1038 (Unlicensed $G_1$) show a similar Mcm2 signal to $G_2$ cells. After a proliferative fate decision has
1039 been made, origins become licensed and cells commit to S-phase entry. Cells enter S-phase
1040 after maximal origin licensing (Active-$G_1$). During S-phase, Mcms are then displaced from
1041 DNA during replication.

1042 (**F**) Representative images of extracted and unextracted intestinal organoids stained with an
1043 antibody against Mcm2 (Red).

1044 (**G**) The Mcm2 labelling index for unextracted and extracted organoids. Data is displayed as
1045 Mean +/- SEM, N = 3 organoids and shows a significant difference (T test, $p<0.0001$).

1046 **Figure 3. The licensing state defines distinct proliferative zones in intestinal crypts**

1047 (**A**) Representative image of an extracted intestinal crypt isolated after a 1 hour EdU pulse *in*
1048 *vivo* (EdU, Green) and stained with Hoechst (Blue) and antibodies against Mcm2 (Red) and
1049 pH-H3 (White). Co-staining shows distinct cell-cycle phases (bottom panels): Licensed cells
1050 committed in $G_1$ (Mcm2(+), EdU(-)); Early (Mcm2(+), EdU(+)) to Late (Mcm2(-), EdU(+)) S-
1051 phase), and mitotic cells (pH-H3(+)). Negative cells represent deeply quiescent ($G_0$),
1052 terminally differentiated cells or cells in $G_1$, which have not made a proliferative fate
1053 decision, remaining unlicensed. The crypt base is to the left of the displayed image.

1054 (**B**) Nuclear volume was estimated in cells at the distinct cell-cycle phases identified
1055 previously: Negative ($G_0$/$G_1$/$G_2$: N =115), $G_1$ Licensed (Mcm(+), EdU(-): N=38), S-phase
1056 (Mcm(+), EdU(+): N=24) and Late-S/$G_2$ (Mcm(-), EdU(+): N=26). Top Panels show
1057 representative examples of each cell-cycle phase and the associated 3D rendered nuclei.
1058 There was a significant difference in the size of Licensed $G_1$, S and Late-S/$G_2$ nuclei (T test,
1059 $p<0.0001$).

1060 (**C**) Representative images of intestinal crypts isolated after a 1 hour EdU pulse (Green) *in*
1061 *vivo*. Displayed are 3D projections of extracted and unextracted crypts stained with Hoechst
1062 (Blue) and an antibody against Mcm2 (Red). The crypt base is to the left of the displayed
1063 image.

1064 (**D**) Comparison between cells expressing Mcm2 protein and DNA-bound Mcm2 along the
1065 crypt-villus axis between unextracted (N=101 crypts) and extracted (N=109 crypts) (taken
1066 from 3 mice). Data is displayed as the mean % of cells per set distance bin.

1067 (**E**) All cells were divided into 4 distinct groups based on Mcm2 and EdU intensities. These
1068 groups represent distinctive cell-cycle phases as defined by their total (unextracted N=101
1069 crypts) or licensed (extracted N=109 crypts) Mcm2 content: **Extracted:** 1) **Unlicensed**
1070 (Mcm2(-), EdU(-)), 2) **$G_1$ licensed** (Mcm2(+), EdU(-)), 3) **Early/Mid S-phase** (Mcm2(+),
1071 EdU(+)) and 4) **Late-S/$G_2$** (Mcm2(-), EdU(+)). The data is represented as the population mean
1072 of the total cells per distance bin, Mean +/- SEM.
1073 (**F**) The distance of the most distal Mcm2(+) and EdU(+) cells to the crypt base was
1074 compared in extracted and unextracted crypts. Data was scored manually for 10
1075 representative crypts per condition. Licensed cells (Mcm2(+)) were significantly closer to the
1076 crypt base than EdU(+) cells (T test, $p=0.0015$. Cells expressing Mcm2 protein extended
1077 significantly above the last EdU(+) cell (T test, $p<0.0003$)

1078 (**G**) Representative images of crypts isolated 17 hours after administration of EdU (Green).
1079 3D projections of extracted and unextracted crypts stained with Hoechst (Blue) and an
1080 antibody against Mcm2 (Red) are shown.

1081 (**H**) Cells were divided into 4 distinct groups as in Panel **E** (N=51 Crypts).

1082

1083 **Figure 4. Intestinal stem cells reside in a paused unlicensed $G_1$**

1084 (**A**) Quantification of cell cycle stages for cells in the stem cell (SC) compartment (<40 µm
1085 from the crypt base) and in the early transit-amplifying (TA) compartment (40-80 µm from
1086 the crypt base), as described in Figure 3E (**N=49 crypts**).

1087 (**B**) Representative image of an extracted crypt base isolated 1 hour after a pulse of EdU
1088 (Green) and stained with Hoechst (Blue), UEA (Red) and antibodies against Mcm2 (White).
1089 Nuclear morphology and UEA signal were used to distinguish between UEA(+) Paneth Cells
1090 (outlined by dashed lines and nuclei marked with blue stars) and UEA(-) stem cells (situated
1091 between outlined Paneth cells and with nuclei marked by red stars).

1092 (**C**) The average % of UEA(-) stem cells that fall into the previously defined cell-cycle bins:
1093 (Unlicensed; $G_1$ licensed; S-phase; S/$G_2$ phase; N=68 crypts).

1094 (**D**) Representative flow cytometry profiles of (**i**) isolated Lgr5$^{Hi}$ intestinal stem cells from 3
1095 mice, showing DNA-bound Mcm2 and DNA content. The 2N ($G_1$) cells of the same
1096 population are also shown (ii). The respective gated populations for Unlicensed $G_1$ (Black),
1097 Licensed (Red), S-phase (Yellow) and $G_2$/M (Green) are shown. The Ki67 content of the
1098 Licensed and Unlicensed $G_1$ cells are also shown (iii).

1099 (**E**) The frequency distribution of mean DNA-bound Mcm2 intensities for Mcm2(+) cells in $G_1$
1100 cells.

1101 (**F**) Simulated ergodic rate analysis of origin licensing during $G_1$. We simulated origin
1102 licensing dynamics during $G_1$, varying the licensing rate and incorporating a significant
1103 paused period (Unlicensed $G_1$). The displayed histograms show the frequency distribution of
1104 DNA-bound Mcm2 of $G_1$ cells. Please refer to materials and methods for further
1105 information. However, an analogy to explain the model is as follows: Origin licensing
1106 through $G_1$ can be thought of in terms of cars travelling along a long stretch of motorway: if
1107 cars enter the motorway at a fixed rate (i.e. unsynchronised cell cycles, cells entering G1)
1108 the density of cars at any one point is inversely proportional to the speed they are travelling
1109 at ('speed' in our case means the rate of licensing). We have added the concept of delays at
1110 the start and end, like tollbooths. In our model, there is a minimum drive time (the
1111 minimum length of $G_1$ required for cells to grow to a critical size before they enter S phase
1112 (arbitrarily set at '100%'). If the speed of the cars means they don't reach the end of the
1113 motorway before this time is up, cars maintain a constant speed along the entire road, and
1114 exit the motorway as soon as they reach the end. If cars drive faster and they reach the end
1115 before this time is up (>100%), they have to wait at the end of the motorway till the critical
1116 time is expired, resulting in a peak accumulation at the fully licensed point. Unlicensed $G_1$ is
1117 an enforced time that cars have to wait once they enter the motorway before they are
1118 allowed to drive along it. This creates a peak on the left (unlicensed cells). If the cars then
1119 drive slowly, when they get to the end of the motorway, they exit immediately because the
1120 critical time has expired (centre panels), **but** if they drive fast enough they reach the end of
1121 the motorway before the critical time has expired. This results in a peak accumulation at
1122 both minimally and maximally licensed points.

1123 (**G**) Comparison of DNA-bound Mcm2 content of Lgr5(+) and Lgr5(-) $G_1$ cells and of cells in
1124 very early S-phase.

1125 **Figure 5. Label retaining cells are in a deep-$G_0$ state**

1126 (**A**) Labelling strategy. H2B-GFP expression was induced in all intestinal epithelial cells in
1127 H2B-GFP mice by administration of doxycycline for 7 days. After complete labelling,
1128 doxycycline was removed and mice rested for 7 days. During this chase period, the majority
1129 of H2B-GFP(+) cells are lost by label dilution due to cell division and upward migration. Both
1130 Paneth cells and +4 Label retaining cells are H2B-GFP(+) after the chase period. +4 Label
1131 retaining cells were distinguished from Paneth cells on the lack of UEA staining (Buczacki et
1132 al., 2013).

1133 (**B**) Representative images of whole-mount sections of H2B-GFP expressing small-intestinal
1134 tissue after a 7-day labelling period (i). A vibratome section (ii) of intestinal tissue after a
1135 subsequent 7-day chase period, stained with Hoechst (nuclei), UEA (Grey), and an antibody
1136 against Mcm2 (Red). An enlarged image of the marked crypt is shown. A UEA(-) label
1137 retaining cell (LRC) is marked by the white arrow). Quantification of the mean GFP intensity
1138 for all cells along the crypt-villus axis after the 7 days chase period is shown (iii).

1139 (**C**) A representative image (i) of a label-retaining cell in an intestinal crypts stained with
1140 Hoechst (Blue), UEA (White) and an antibody against Mcm2 (Red). The label retaining cell
1141 (White arrow) does not express Mcm2. The quantification of Mcm2 expression in label
1142 retaining cells (N=12), Paneth cells (N= 116) and all cells (N=543) is shown (iii).

1143 (**D**) Representative images of extracted H2B-GFP crypts after the 7-Day chase period. H2B-
1144 $GFP^{Hi}$ cells (bright Green) represent Paneth cells and +4 cells (i), and H2B-$GFP^{Low}$ cells (Faint
1145 Green) represent daughter cells (white arrow) that have diluted H2B-GFP content as a result
1146 of cell division (ii). The quantification of DNA-bound Mcm2 in $GFP^{Hi}$ label retaining (LR) and
1147 $GFP^{low}$ daughter cells compared with the total cell population (all cells) is shown (iii).

1148 **Figure 6. Licensing dynamics in intestinal organoids**

1149 (**A**) Representative image of an unextracted and extracted intestinal organoid stained with
1150 Hoechst (Blue), and an antibody against Mcm2 (Red) after a 1 hour EdU pulse (green).

1151 (**B**) Representative flow cytometry profiles from isolated organoids cells showing Ki67 (i) or
1152 DNA-bound Mcm2 (ii) content vs DNA content.

1153 (**C**) Representative flow cytometry profile from cells isolated from cultured organoids (i) or
1154 intestinal crypts (ii) showing DNA-bound Mcm2 vs Ki67 (**See also S5 Figure A**). Ki67 loss and
1155 subsequent loss of Mcm2 during differentiation is apparent, starting from Unlicensed $G_1$
1156 (dashed arrow). Quantification of discrete populations (gates shown in i) was performed: 1)
1157 $G_0$, 2) Transition ($G_0 \leftrightarrow$ Unlicensed $G_1$), 3) Unlicensed $G_1$, 4) Licensed $G_1$, 5) S-Phase, 6) Late-
1158 $S/G_2/M$. (N=3).

1159 (**D**) Representative flow cytometry profiles of isolated organoid epithelial cells grown in ENR
1160 (control) and treated with the EGFR inhibitor Gefitinib, for the indicated times (**i-iii**). After 4
1161 Days in Gefitinib, organoids were reactivated by removal of the Gefitinib and re-addition of
1162 fresh growth factors (ENR) for 2 days (**iv**). Displayed are profiles comparing DNA-bound
1163 Mcm2 vs Ki67 (Top panels) or total Mcm2 content (Bottom panels).

1164 (**E**) The $G_1$ cell populations as shown in (D) were quantified. DNA-bound Mcm2 profiles (i)
1165 show 1) Unlicensed $G_1$, 2) Licensed $G_1$, 3) Transition ($G_0 \leftrightarrow$ Unlicensed $G_1$), 4) $G_0$ populations.
1166 Total-Mcm2 profiles (ii) show Mcm2 expressing (Mcm2(+)) and non-expressing (Mcm2(-))
1167 Cells. (N=3 organoids)
1168

1169 **Figure 7. Unlicensed $G_1$ is lost in *Apc* mutant epithelium**

1170 (**A**) A representative vibratome section of $Apc^{Min/+}$ intestinal epithelium stained with
1171 Hoechst (nuclei), Phalloidin and an antibody against Mcm2. Regions of normal histology and
1172 a region containing a polyp are highlighted.

1173 (**B**) Representative image of an extracted $Apc^{Min/+}$ isolated crypt (i) stained with Hoechst
1174 (Nuclei) and an antibody against Mcm2 (Red), after a 1 hour EdU pulse (Green). A
1175 representative image of an abnormally elongated crypt is displayed (ii) showing a clonal
1176 ribbon of cells in the distal transit-amplifying compartment which are EdU(+). Quantification
1177 of cell-cycle stages across the crypt axis (Figure 3) is shown (iii).

1178 (**C**) Representative bright field images of organoids cultured from wild-type and organoids
1179 from $Apc^{Min/+}$ mice that have undergone loss of heterozygosity ($Apc^{Min/Min}$).

1180 (**D**) Representative images of unextracted and extracted $Apc^{Min/Min}$ organoids stained with
1181 Hoechst (nuclei), an antibody against Mcm2 (red), after a 1 hour EdU pulse.

1182 (**E**) Representative flow cytometry profiles from cells from extracted wild-type and $Apc^{Min/Min}$
1183 organoids showing DNA-bound Mcm2 vs DNA content (i). The 2N $G_1$ cells of the shown
1184 profile are displayed (ii) showing Unlicensed $G_1$, Early $G_1$ and Peak (fully licensed) $G_1$
1185 populations.

1186 (**F**) Quantification of the populations described in Panel Eii. Data is displayed as mean +/-
1187 SEM, N=3 organoids.

1188 (**G**) Western blot of RB and pRB (low and high exposures) levels between wild-type and
1189 $Apc^{Min/Min}$ organoids. Two bands corresponding to hypo- and hyper-phospohorylated RB can
1190 be observed.

1191 (**H**) Quantification of the fold increase of pRB:RB for $Apc^{Min/Min}$ organoids (N=3) and polps
1192 isolated from $Apc^{Min/+}$ mice (N=6), compared to *wild-type* organoids and tissue.

1193

1194 **Figure 8. Model of Origin licensing dynamics in intestinal epithelial cells**

1195 In a normal cell-cycle, Mcms are expressed ubiquitously in all stages. The licensing of DNA
1196 with MCM2-7 occurs in late M and throughout $G_{1,}$ when a cell receives a stimulus to commit
1197 to the cell cycle. As DNA is replicated during S-phase, MCM2-7s are displaced from DNA and
1198 are prevented from relicensing in $G_2$. During terminal differentiation, MCM2-7 are not
1199 actively transcribed and the proteins are gradually lost in post-mitotic cells. However, after
1200 the final mitotic division, cells make a binary decision never to license their DNA, even
1201 though the protein is still present. Mcm proteins then degrade slowly, where cells enter a
1202 terminally differentiated state (deep $G_0$). Alternatively, cells can exit mitosis, not relicense
1203 their DNA but maintain proliferative markers and disengage from the cell cycle for some
1204 time (Unlicensed $G_1$). Two major classes of intestinal stem cells exist: 'Active' stem cells,
1205 engaged with the cell-cycle, and reserve, quiescent Label Retaining Cells. Label retaining
1206 cells are in a state of 'deep' quiescence, and do not contain MCM2-7 because they have
1207 disengaged from the cell cycle for some time. In this study, we show that most 'Active'
1208 Lgr5(+) stem cells reside in an unlicensed state, but contain MCM2-7 proteins. These cells
1209 reside in an 'Unlicensed-$G_1$' until they make a proliferative fate decision, enter the cell-cycle
1210 and license. This provides an explanation for the elongated cell-cycle of Intestinal stem cells:
1211 They reside in a partial resting state where they may be able to respond to niche cues to
1212 divide. This therefore may constitute a unique mechanism to control stem cell numbers.

1213 **Supplementary Figure Legends**

1214 **S1 Figure. Image analysis**

1215 (**A**) Image analysis work-flow.

1216 (**B**) Representative image of an extracted isolated crypt 1 hour after an EdU pulse (Green)
1217 stained with Hoechst (Blue) and an antibody against Mcm2 (Red).

1218 (**C**) Detection of nuclei in the crypt in panel A in 3D. Nuclei were detected in 3D using
1219 segmentation tools in Imaris. Detection was validated visually or each individual crypt.

1220 (**D**) Segmentation of the region of interest defined by nuclei detection in panel B.

1221 (**E**) A distance transform was performed in Imaris to measure the distance of each nucleus
1222 to a reference nucleus at the crypt base. Visual representations of distances divided into
1223 different bins are displayed (Green, 0-10µm; Yellow, 10-20 µm; Red, 20-30µm; Blue, 30-
1224 40µm; Magenta, 40-50µm).

1225 (**F**) Representative 3D quantification of the crypt in panel A shows the distance from the
1226 crypt base (X-axis), DNA-bound Mcm2 (Y-axis) and EdU incorporation (Z-axis).

1227 (**G**) An overview of the gating strategy used for flow cytometry experiments. Intestinal
1228 epithelial cells were separated from debris on the basis of forward and side scatter. Single
1229 cells were subsequently distinguished from doublets based on pulse-width gating. Negative
1230 gates were set on control samples stained with secondary antibody alone. Unlicensed $G_1$
1231 (Population 1) and licensed-$G_1$ (Population 2) were distinguished based on DNA-content and
1232 based on the threshold set by the negative control samples. S-phase cells (Population 3) can
1233 be seen as an arc of cells emanating from the fully licensed cell population, increasing in
1234 DNA content whilst losing DNA-bound Mcm2. $G_2$/M cells (Population 4) can be seen as a
1235 population with 4N DNA content and lacking DNA-bound Mcm2.

1236 **S2 Figure. Clonal cell-cycle patterns in the intestinal epithelium**

1237 (**A**) Representative section through an extracted crypt after a 1 hour EdU pulse (Green) and
1238 stained with Hoechst (Blue) and an antibody against Mcm2 (Red). Discrimination of cell-
1239 cycle staging using DNA-bound Mcm2 and EdU incorporation patterns allows visualisation of
1240 clonal cell-cycle field effects revealing many neighbouring cells with similar DNA-bound
1241 Mcm2 and DNA replication patterns. These clones may represent lineages of from single
1242 cells that progress through the cell cycle at the same rate.

1243 (**B**) Representative image of an isolated crypt in which surface rendering was performed on
1244 all nuclei and colour codes applied to reflect cell-cycle stage. Representative cell-cycle
1245 distributions for isolated Ki67(+), Lgr5(+) and Lgr5(-) intestinal epithelial cells are shown.

1246 (**C**) Representative cell-cycle distributions for isolated Ki67(+), Lgr5(+) and Lgr5(-) intestinal
1247 epithelial cells. The average of each cell-cycle phase is displayed for duplicate isolations.

1248 (**D**) Nuclear volumes were rendered for individual nuclei in whole intestinal crypts isolated 1
1249 hour after labelling with EdU. Image shows nuclei (Blue), EdU (Green) and licensed Mcm2
1250 (Red). Maximum intensity projections of the original image are displayed at the top and
1251 corresponding rendered nuclei at the bottom. Nuclear surfaces were colour-coded
1252 according to cell-cycle states: Blue, unlicensed; Red, Licensed $G_1$; Yellow, S-phase; Green,
1253 Late-S/$G_2$. Nuclear volumes were measured for all nuclei in representative crypts (N=3).
1254 Unlicensed (N=368); $G_1$ (N=104); S-phase (N=41); Late-S/$G_2$ (N=70) and the distance of cells
1255 from the crypt base were binned into 10µm intervals. Known parameters of the nuclear
1256 volume for known cell-cycle stages (Figure 3B) are overlaid.

1257

1258 **S3 Figure. Ki67 expression along the crypt-villus axis**

1259 **(A**) A representative isolated crypt 1 hour after labelling with EdU (Green) and stained with
1260 an antibody against Ki67 (magenta)

1261 (**B**) Quantification of the distribution of Ki67(+) cells along the crypt axis. Cells were binned
1262 into four groups: Negative (Ki67(-), EdU(-)); Ki67(+), EdU(-); Ki67(+), EdU(+) and Ki67(-),
1263 (EdU(+) and by their distance from the crypt base. Data is displayed as the average
1264 percentage of a particular cell subtype, per distance bin. Data is displayed as Mean +/- SEM.
1265 Data from 75 crypts is displayed, N = 14,264 cells.

1266

1267 **S4 Figure. Delayed accumulation of Fucci2aR reporter hCdt1(30-120) in intestinal stem**
1268 **cells**

1269 (**A**) Representative image of a vibratome section of intestinal tissue derived from Fucci2aR
1270 mice, stained with Hoechst (Nuclei), an antibody against Mcm2 and showing expression of
1271 the $G_1$ marker hCdt1(30-120) and $S/G_2/M$ marker hGeminin(1/110).

1272 (**B**) Representative images hCdt1(30-120) expression in the crypt base (left panels) and villi
1273 (right panels). Most cells in the crypt base that highly express hCdt1(30-120) are UEA(+)
1274 Paneth cells.

1275 (**C**) A representative image of a Fucci2aR intestinal crypt stained with Hoecsht and and
1276 antibody against Mcm2. All Mcm2(-) Paneth cells (PC) in the crypt base express high levels
1277 of hCdt1(30-120). Most Mcm2(+) stem cells in the crypt base express very low levels of
1278 hCdt1(30-120) ($hCdt1^{low}$). Only few Mcm2(+) cells were found to express high levels of
1279 hCdt1(30-120) ($hCdt1^{High}$). Many cells in the transit-amplifying compartment expressed
1280 hGeminin(1/110).

1281 (**D**) Quantification of the expression of Mcm2, hCdt1(30/120) and hGeminin(1/110) in
1282 Mcm2(+) and Mcm2(-) cells in the stem cell and transit-amplifying compartment. Data is
1283 displayed as a ratio of signal to the background signal detected in negative cells (Stem cell
1284 compartment: Mcm2(+) N=220, Mcm2(-) N=112; Transit-amplifying compartment: Mcm2(+)
1285 N=383, Mcm2(-) N=18).

1286

1287 **S5 Figure. Manipulation of the stem cell niche can artificially induce Unlicensed-$G_1$**

1288 (**A**) Representative flow cytometry profile of extracted epithelial cells isolated from
1289 organoids in ENR media. The displayed image is the same profile displayed in Figure 5C. The
1290 populations in boxed regions 1-7 are overlaid onto the individual Mcm2 and Ki67 cell-cycle
1291 profiles plotted against DNA-content (right hand box).

1292 (**B**) Representative bright-field images of organoids in normal (ENR) media, treated with
1293 Gefitinib for 4 days, and after 2 days in fresh ENR media post Gefitinib treatment.

1294 (**C**) Representative flow cytometry profiles from extracted cells isolated from organoids
1295 treated with 10µM Chir99021 for the indicated time intervals, and after 2 days in fresh ENR
1296 media post Chir99021 treatment.

1297 (**D**) Representative flow cytometry profiles from extracted cells isolated from organoids
1298 treated with normal media (ENR) or in normal media containing Chir99021 and valproic acid
1299 (ENR-CV). Displayed is the comparison of DNA-bound Mcm2 vs Ki67 content (i). The gated
1300 populations: 1) Transition (Unlicensed-$G_1$↔ intermediate $G_0$), 2) Ki67 independent origin
1301 licensing pathway, 3) Fully licensed $G_1$ cells, 4) Normal Licensing, 5) Unlicensed $G_1$ have
1302 been quantified (N=3).

1303 (**E**) Representative images of Lgr5-GFP organoids treated with ENR or ENR-CV. In ENR-CV
1304 treated organoids, the majority of cells express Lgr5.

1305 (**F**) Representative flow cytometry profiles from extracted cells isolated from organoids
1306 treated with Valproic acid for indicated time intervals, and after 2 days in fresh ENR media
1307 post Valproic acid treatment.
1308
1309 (**G**) Representative flow cytometry profiles from extracted cells isolated from organoids
1310 treated with DAPT for indicated time intervals, and after 2 days in fresh ENR media post
1311 DAPT treatment.

1312 (**H**) Representative images of *wild-type* and *Apc*$^{Min/Min}$ intestinal organoids after treatment
1313 with 5µM Gefitinib for 3 days.
1314
1315 (**I**) Model for the unique cell-cycle characteristics of organoid epithelial cells.
1316 Normal, highly proliferative cells, express Ki67 and Mcm2 protein that is not DNA-bound (**1**).
1317 During a normal cell-cycle, cells are activated from Unlicensed-$G_1$, and rapidly license origins
1318 (**2**). Mcms are subsequently displaced during DNA replication (**3**) and remain unlicensed
1319 through $G_2$ (**3**). Inhibiting EGFR causes highly proliferative cells (Ki67$^{hi}$) to arrest in
1320 Unlicensed-$G_1$ with maintained Mcm2 protein expression. Prolonged EGFRi treatment
1321 causes transition into an intermediate state of $G_0$ accompanied by loss of Ki67 expression
1322 (Ki67$^{lo}$), but maintenance of MCM2-7 protein expression (**4**). Induction of terminal
1323 differentiation by inhibition of Notch signalling is associated with a terminal loss of MCM2-7
1324 proteins, and entry into deep-$G_0$ (**5**). Notch activation (or HDAC inhibition (HDACi)) induces a
1325 unique subset of Ki67$^{lo}$ Unlicensed-$G_1$ cells to license origins independently of Ki67 **6**). We
1326 suggest that the unique cell population observed upon ENR-CV / ENR-V treatment may be a
1327 reserve subset of stem cells that express Lgr5 and start expressing MCM2-7 and enter

1328 Unlicensed-$G_1$ from deep-$G_0$. These cells have unique cell cycle characteristics, and can
1329 immediately license origins independently of Ki67 expression (6→2→3).
1330
1331 **S1 Movie. Cell-cycle clones**
1332
1333 A 3D rotation of a representative intestinal crypt showing nuclei (Blue), DNA-bound Mcm2
1334 (Red) and EdU (Green; 1 hour pulse). The crypt base is at the bottom of the image. An
1335 isosurface rendering of nuclei within the crypt has also been performed, and have been
1336 coloured to match specific cell-cycle stage: Unlicensed (Blue), $G_1$ Licensed (Red), Early S-
1337 phase (Yellow), Late S/$G_2$ (Green).
1338

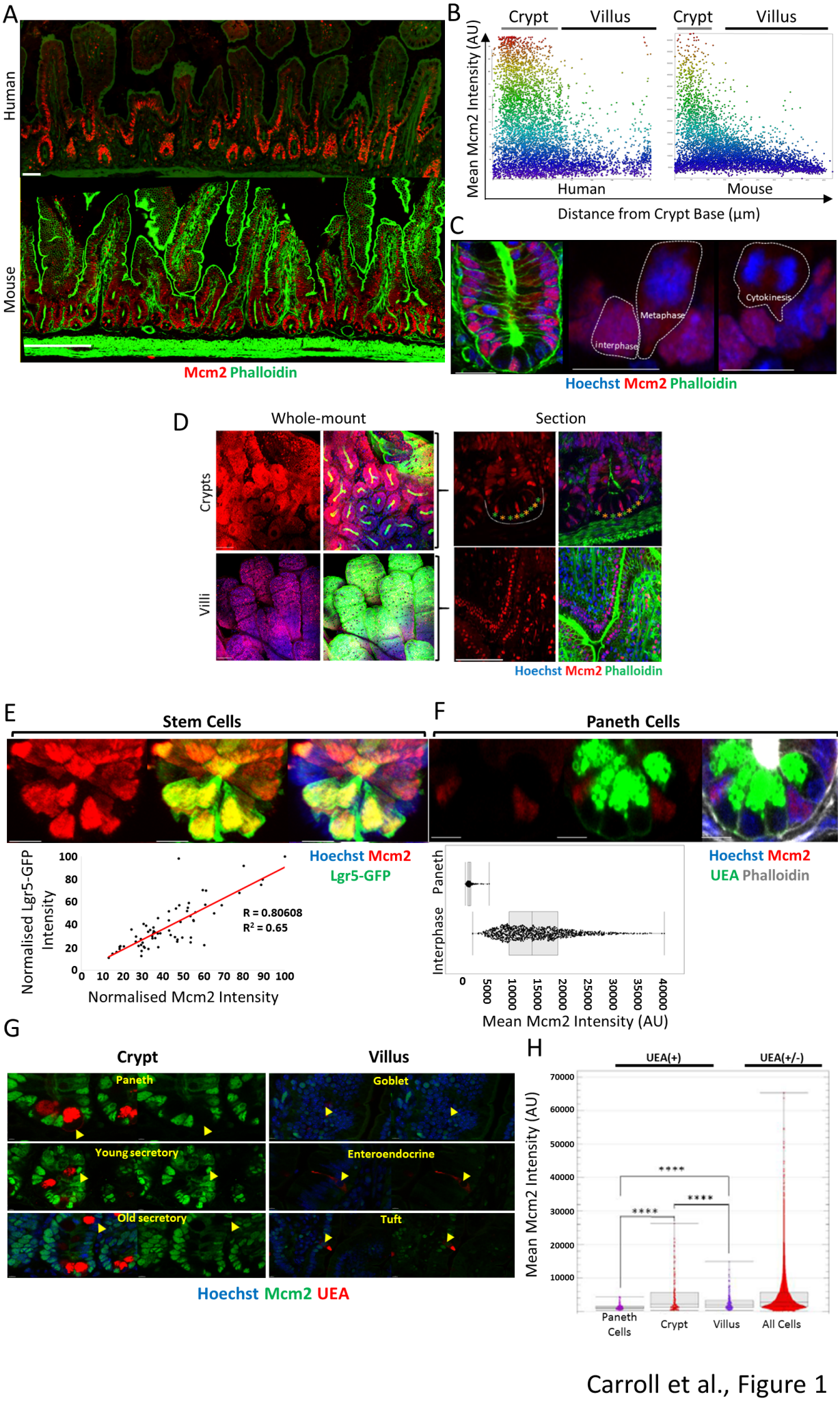


Carroll et al., Figure 1

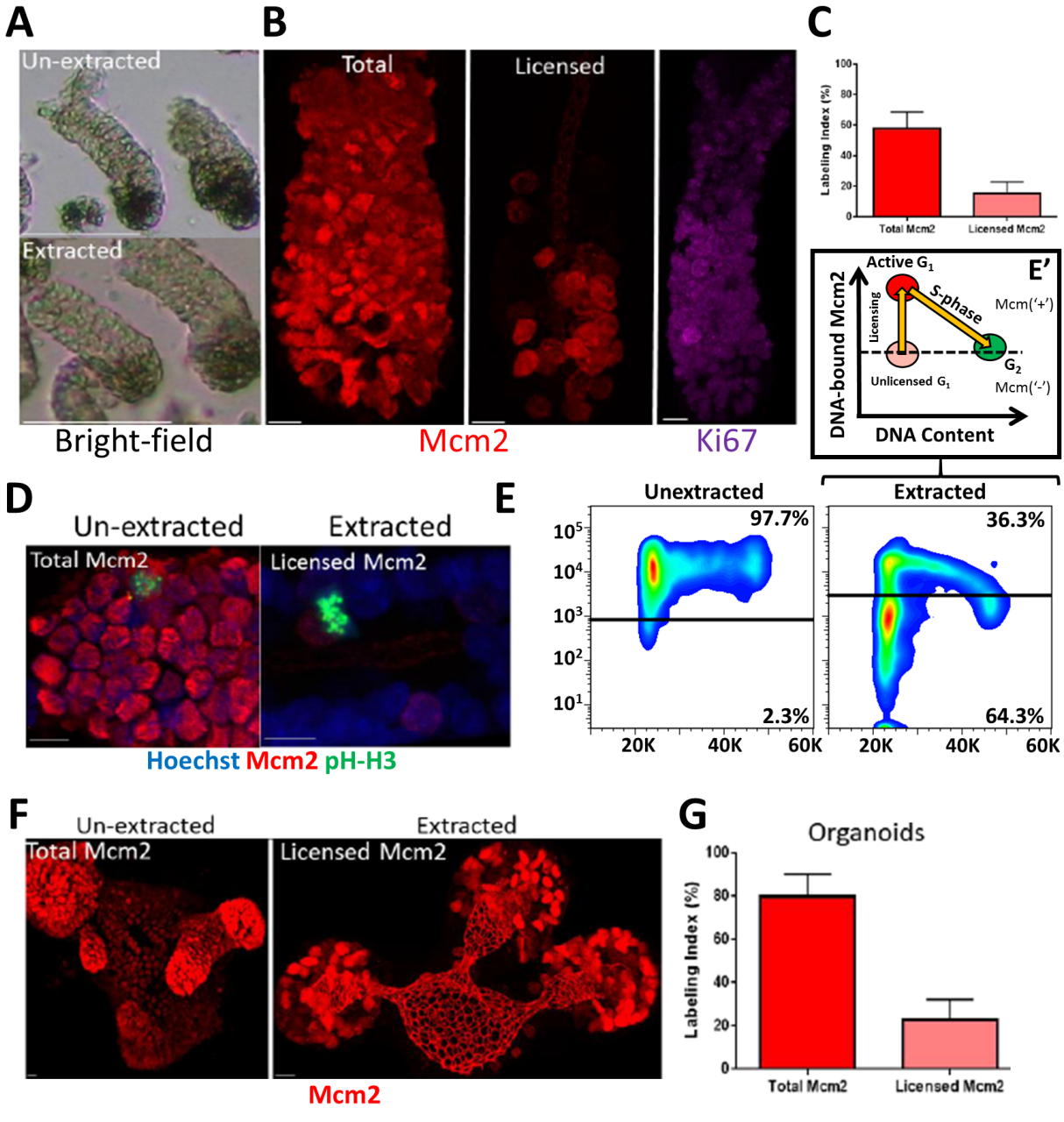


Carroll et al., Figure 2

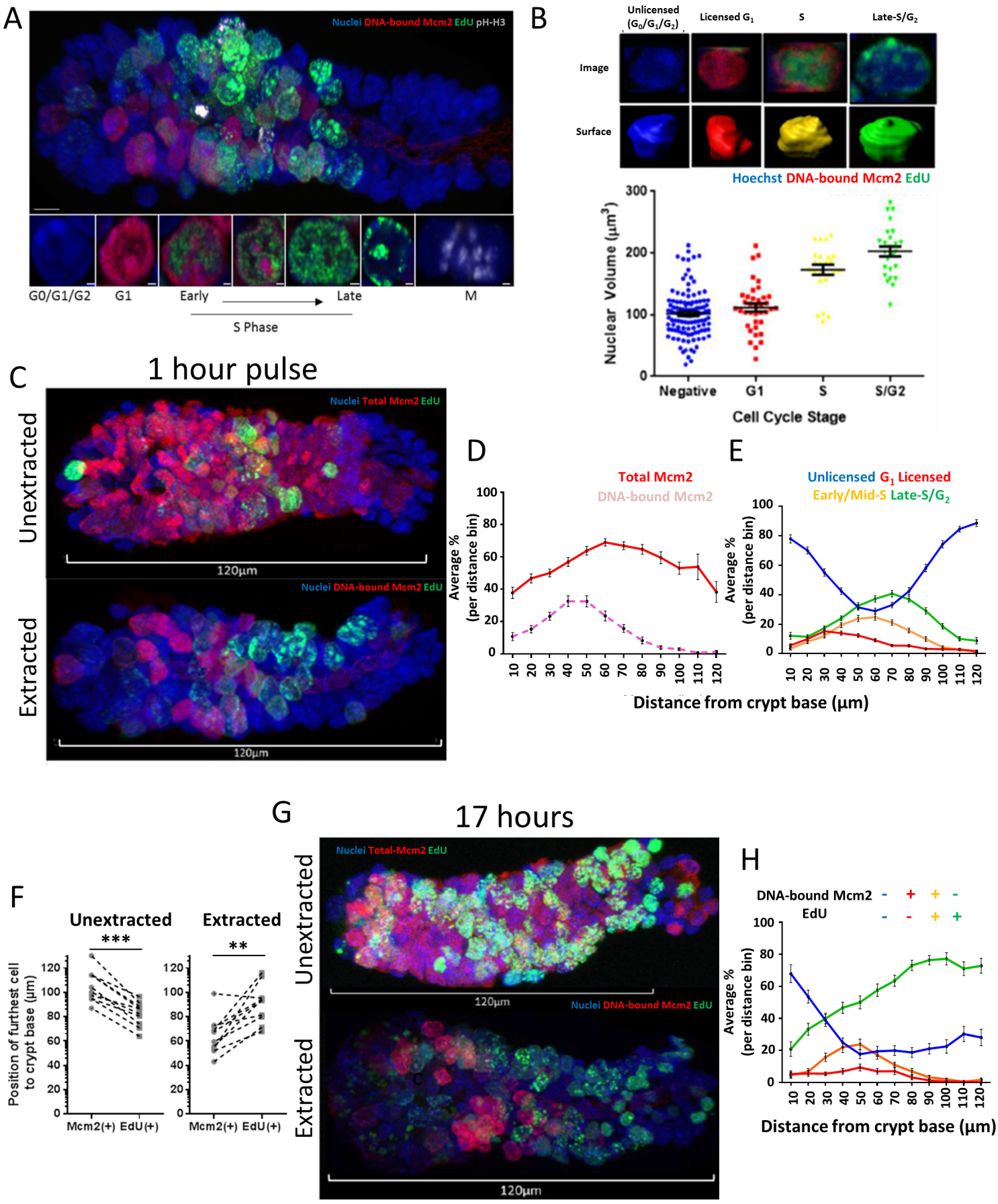


Carroll et al., Figure 3

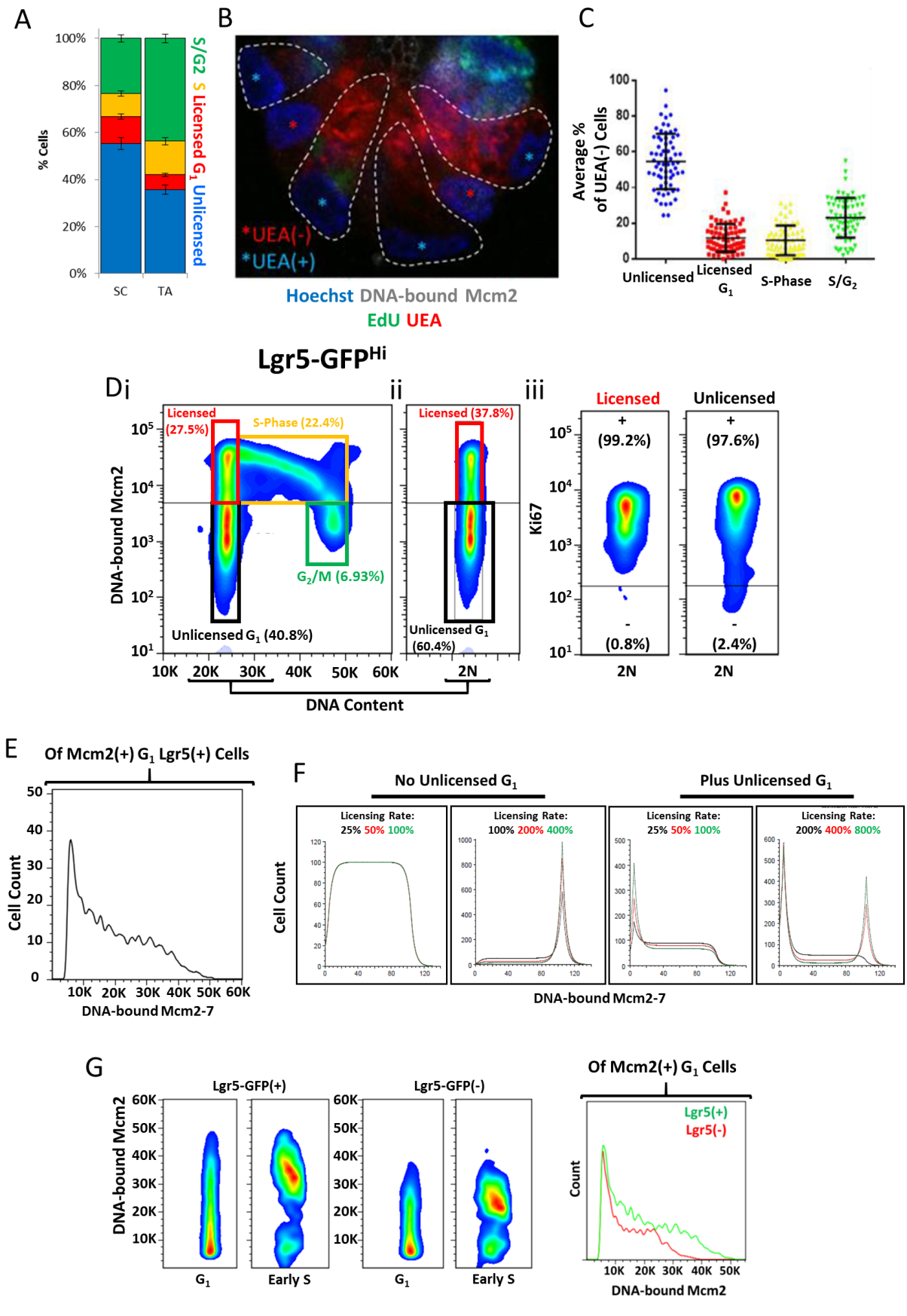


Carroll et al., Figure 4

A

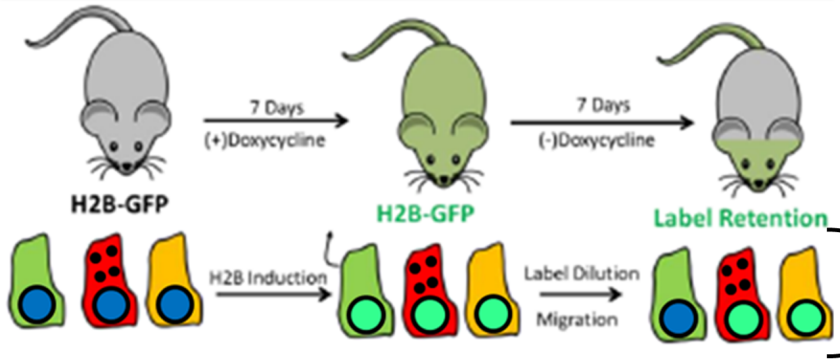


| | SC/TA | Paneth | LRC |
|---|---|---|---|
| H2B-GFP | - | + | + |
| UEA | - | + | - |

Bi

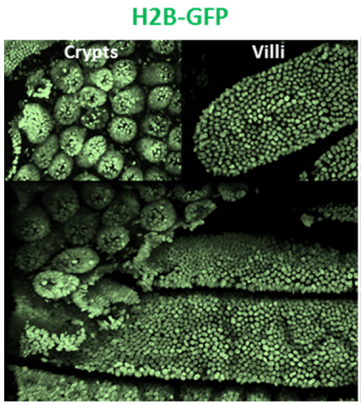


7 Day Induction

ii

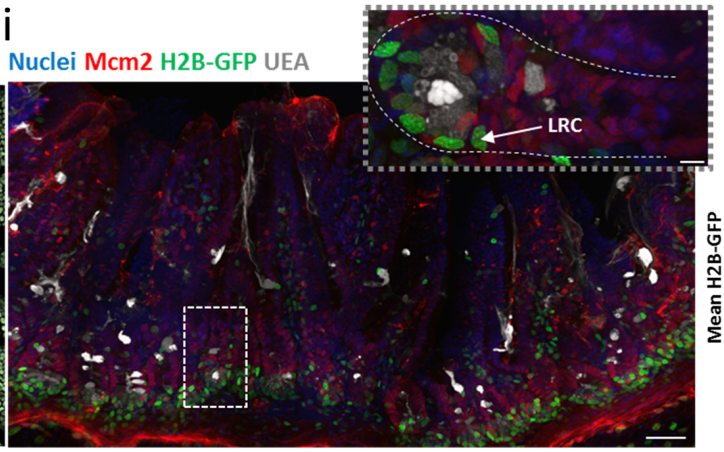


+7 Day Chase

iii

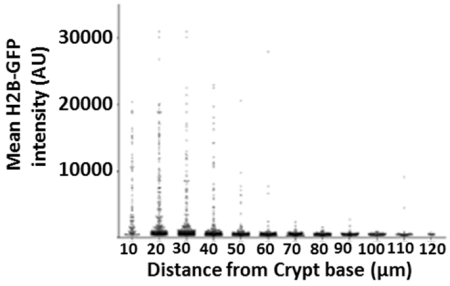


Ci

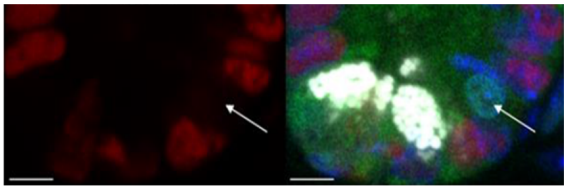


ii

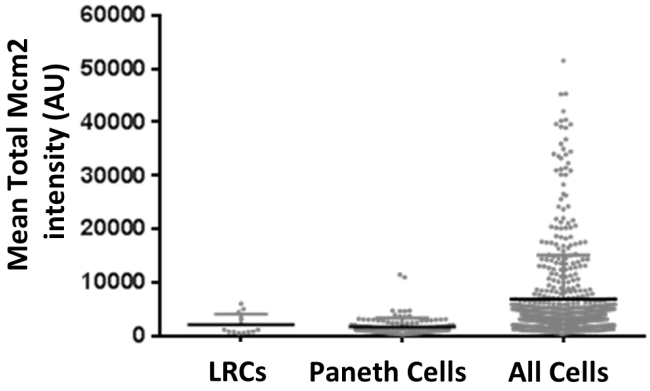


D

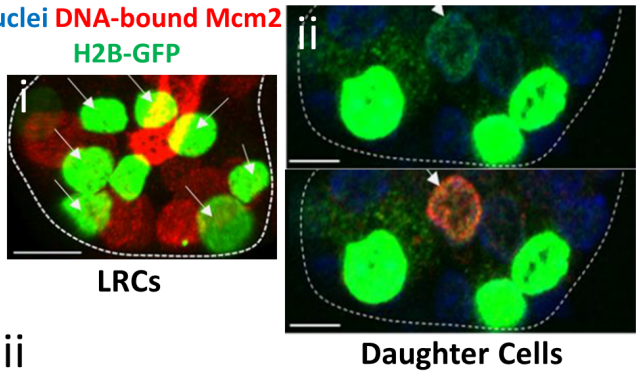


iii

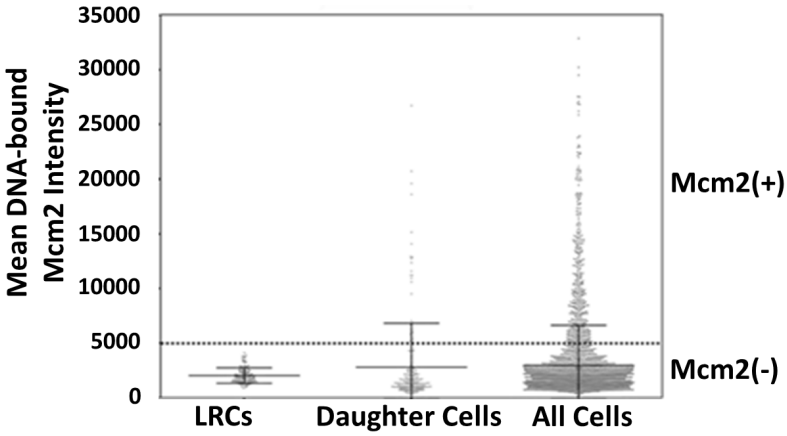


Carroll et al., Figure 5

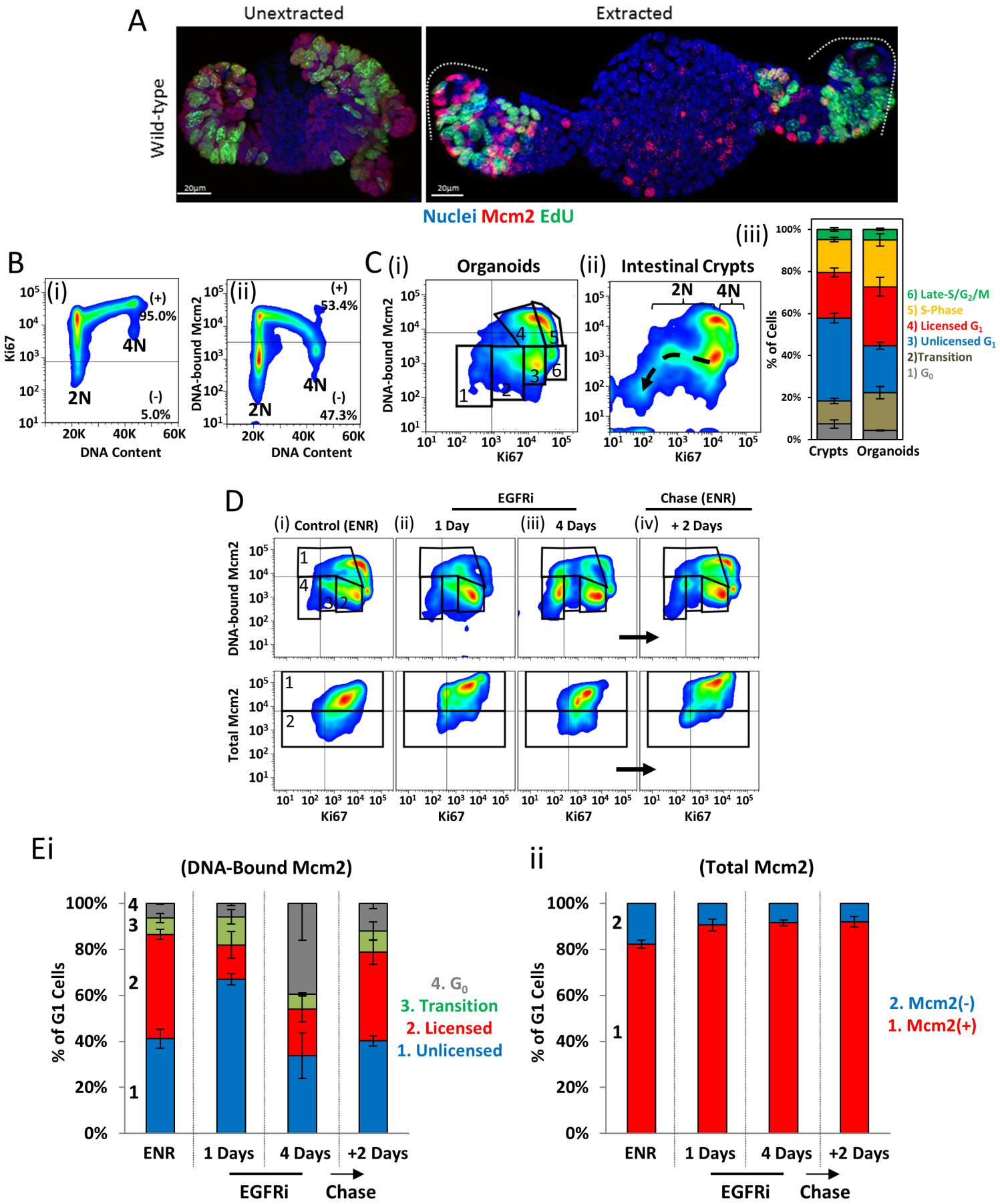


Carroll et al., Figure 6

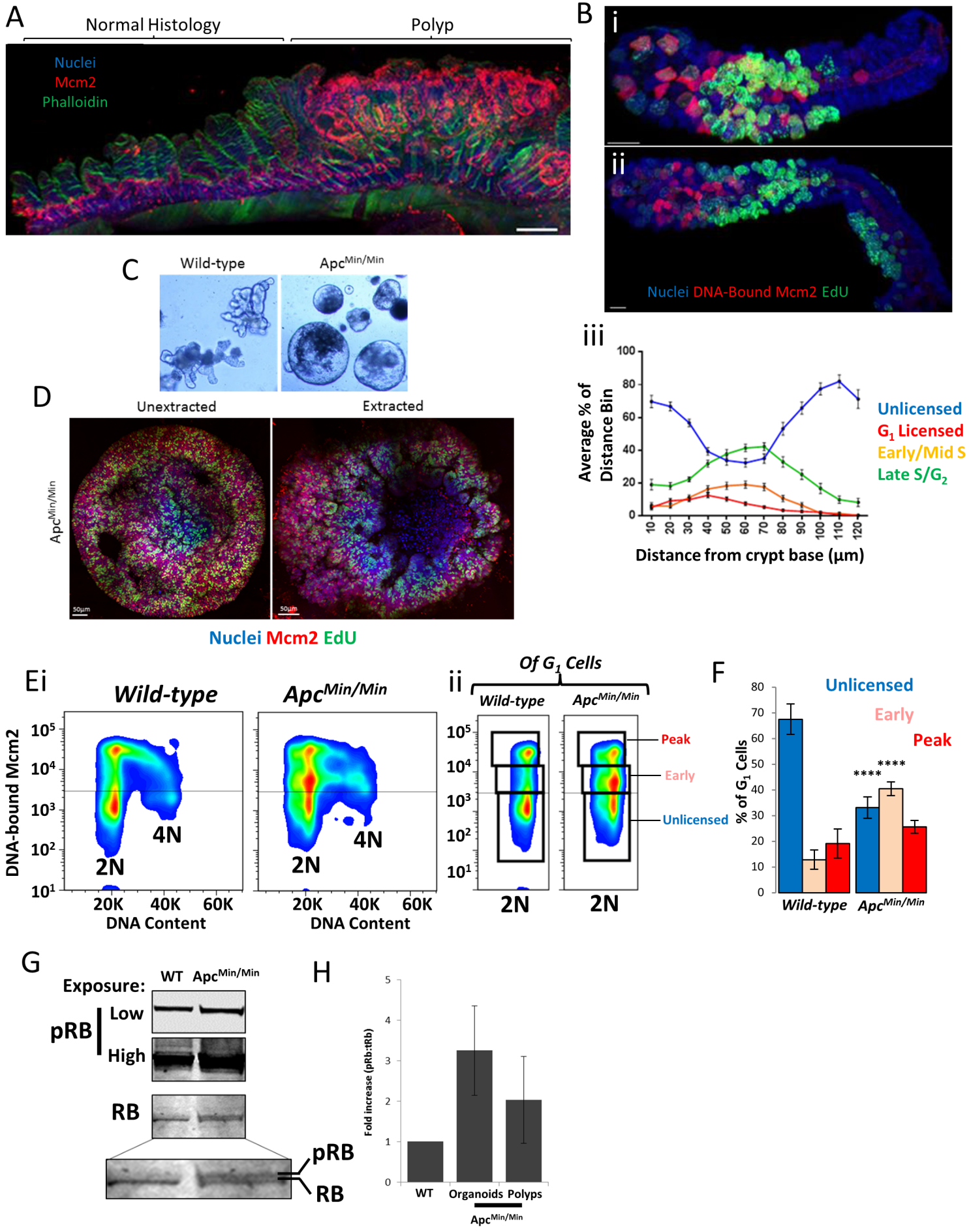


Carroll et al., Figure 7

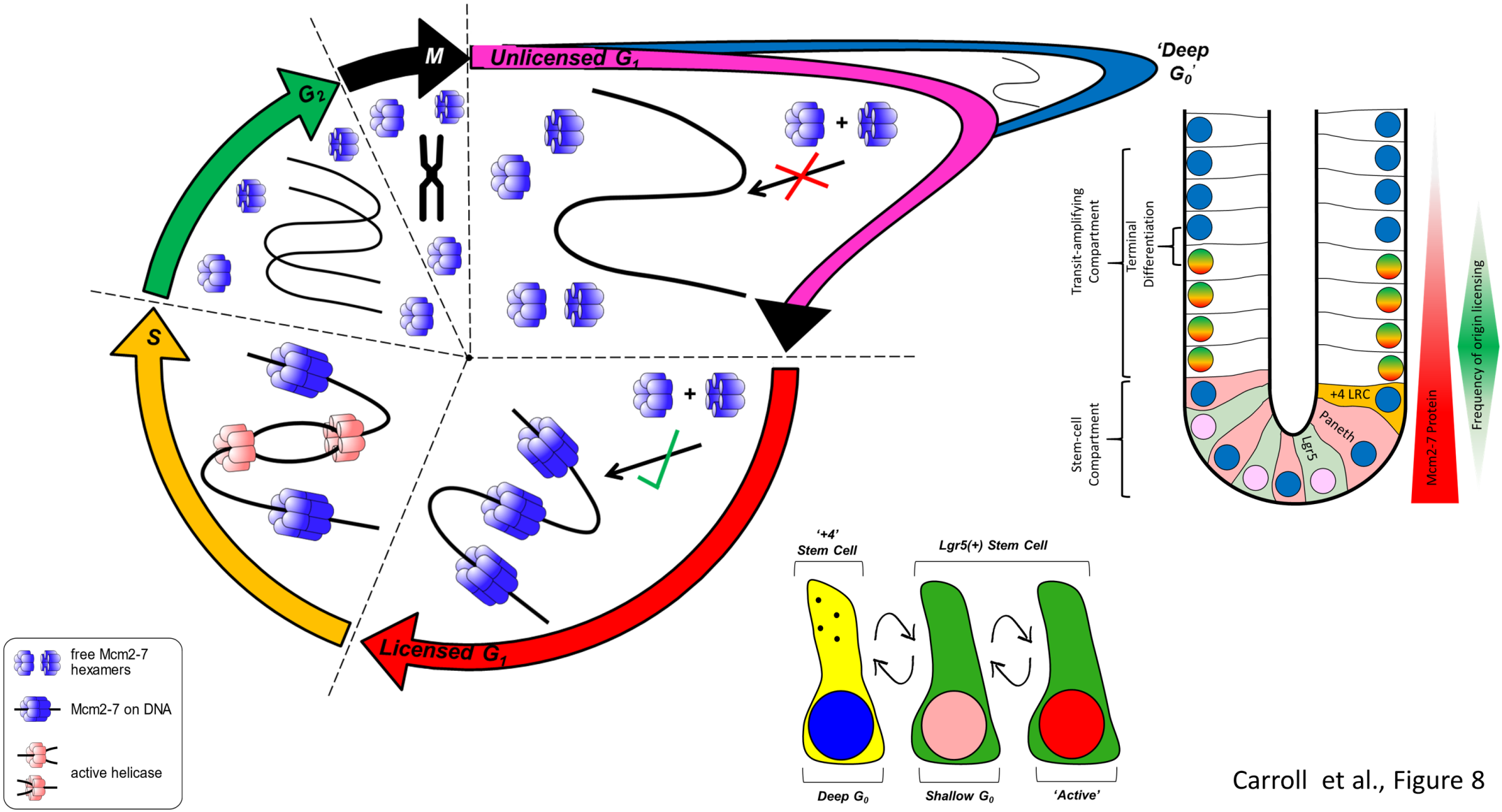


Carroll et al., Figure 8

A

Image acquisition and cropping → Automated detection of nuclei → Manual detection of nuclei → Segmentation → Distance transform → Quantification

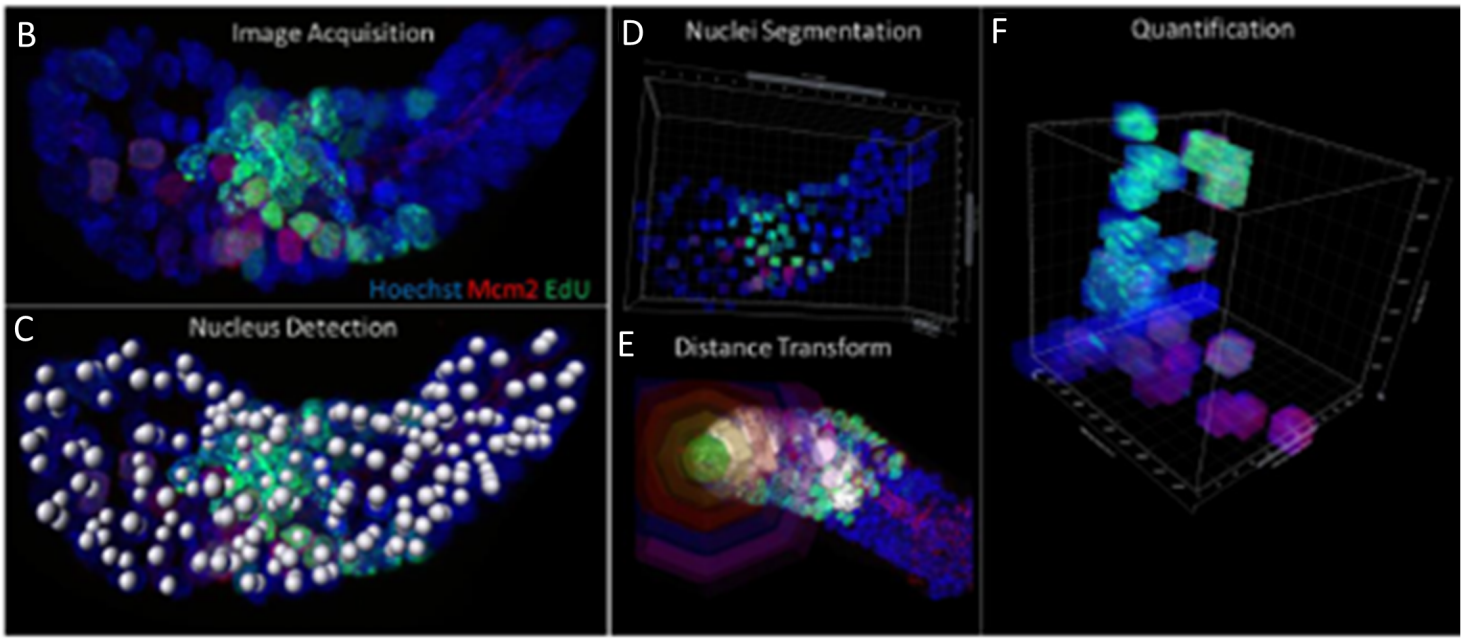


G

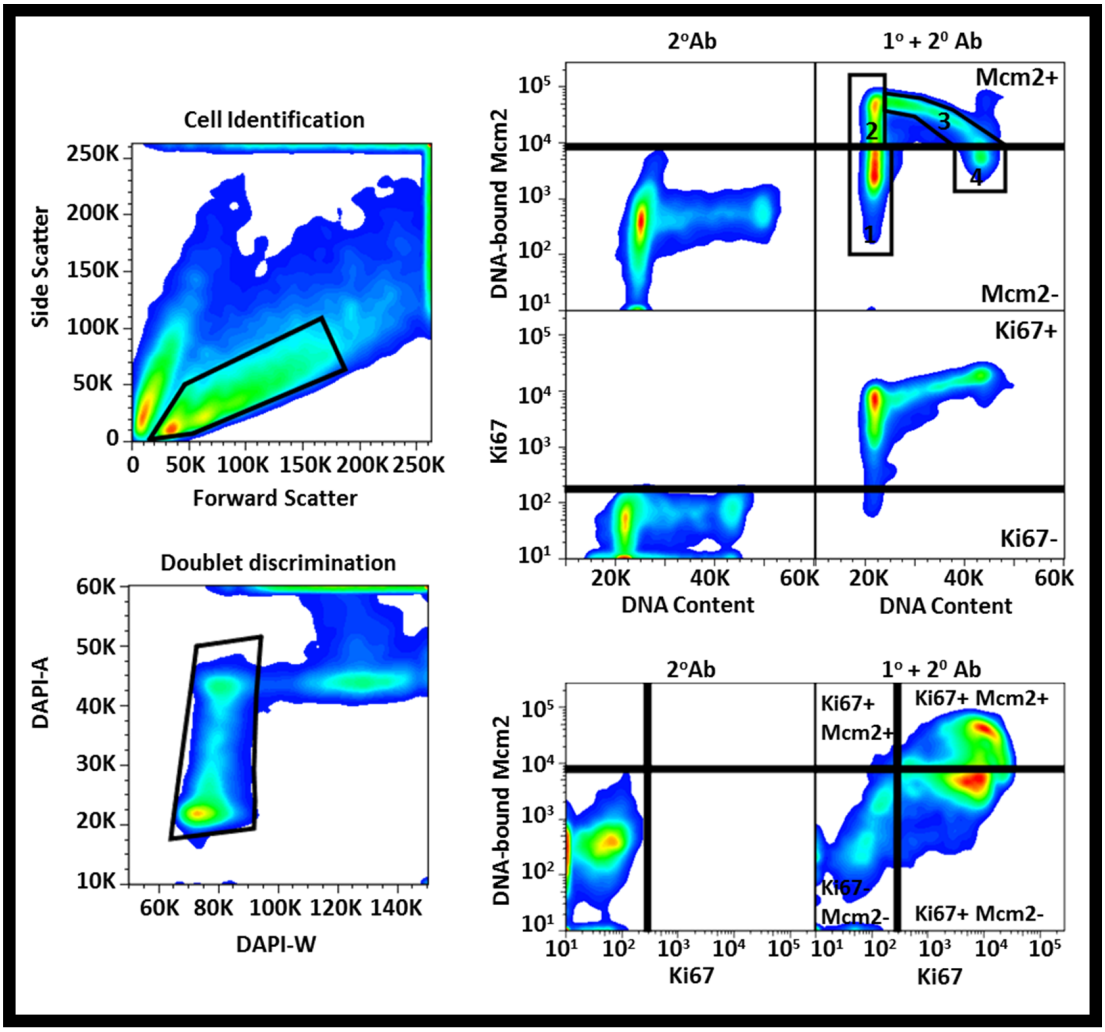


Carroll et al., S1 Figure

A

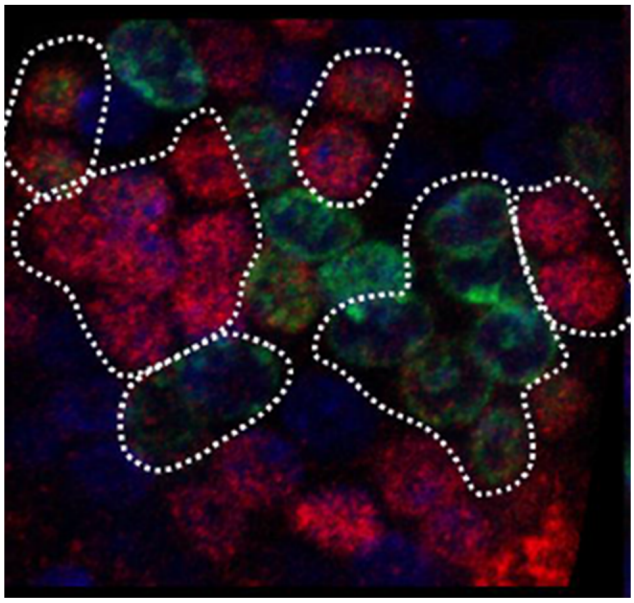

Hoechst DNA-bound Mcm2
EdU (1 Hour pulse)

B

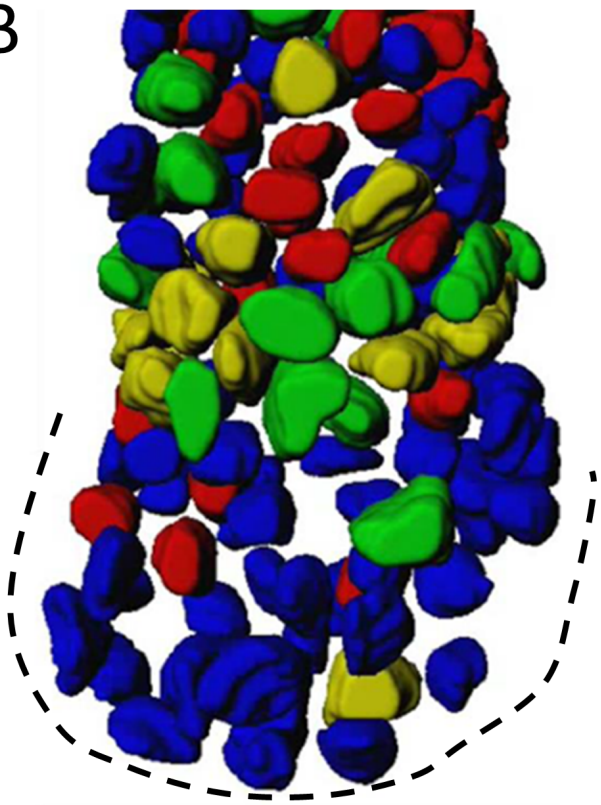

Unlicensed $G_1$ Licensed
Early/Mid S Late-S/$G_2$

C

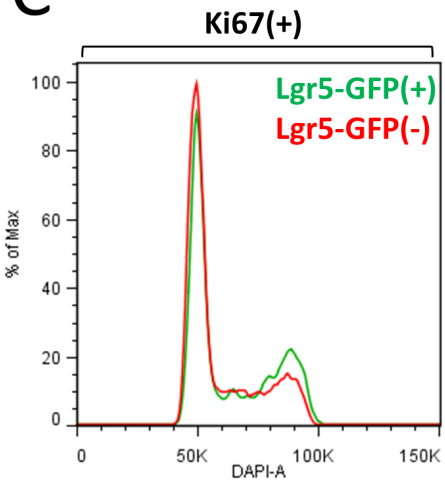


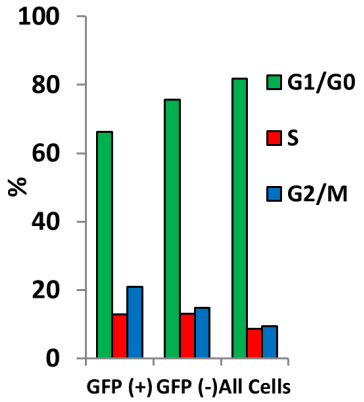


D

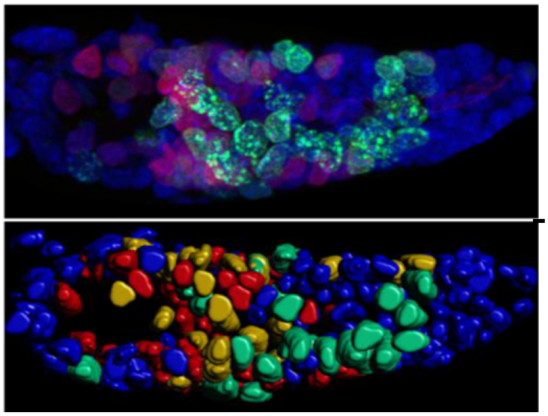

Hoechst
DNA-bound Mcm2
EdU

Unlicensed
$G_1$ Licensed
Early/Mid S
Late-S/$G_2$

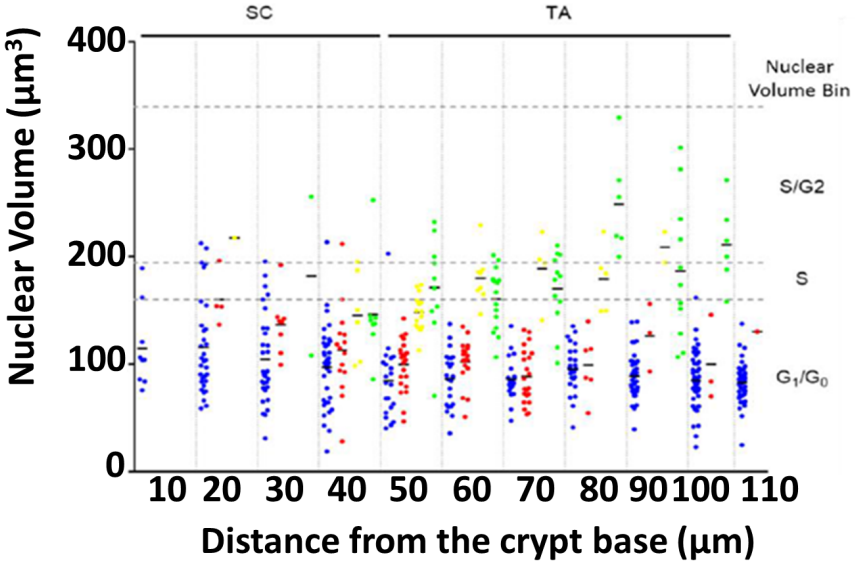


Staining pattern: Unlicensed $G_1$ Licensed
Early/Mid S Late-S/$G_2$

Carroll et al., S2 Figure

# 1 Hour pulse

A

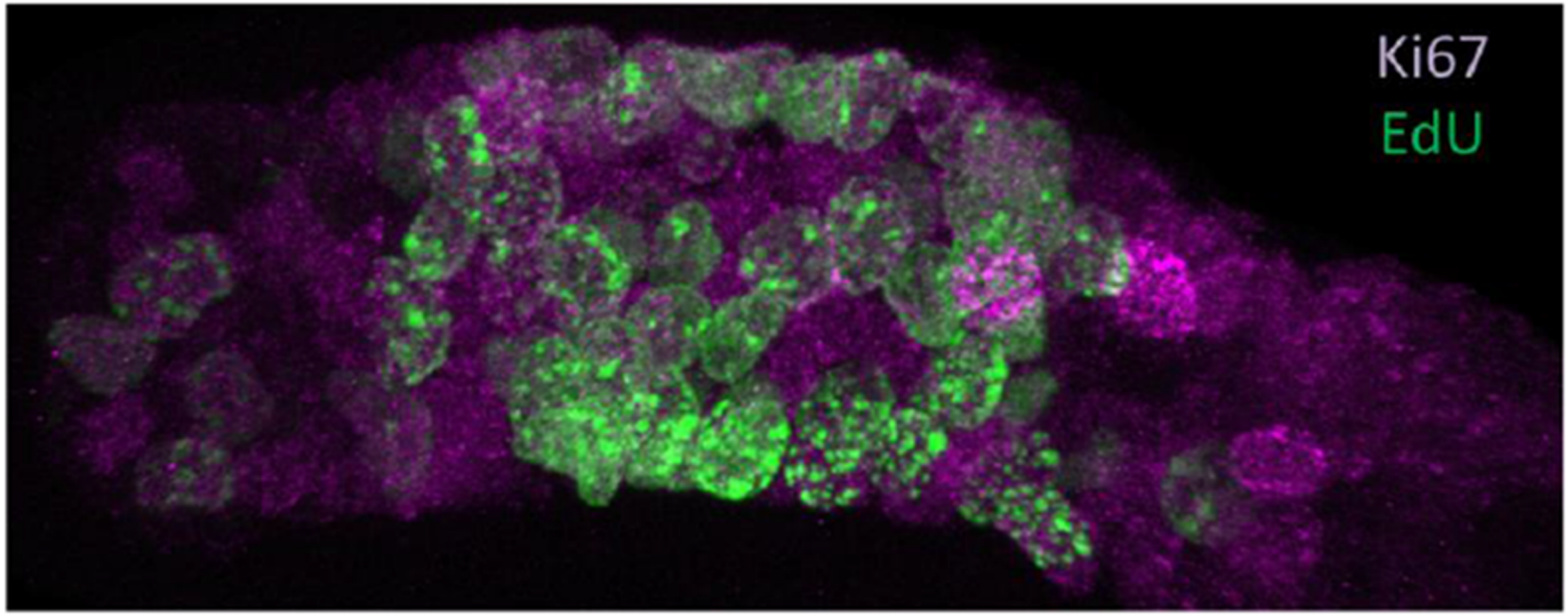


B

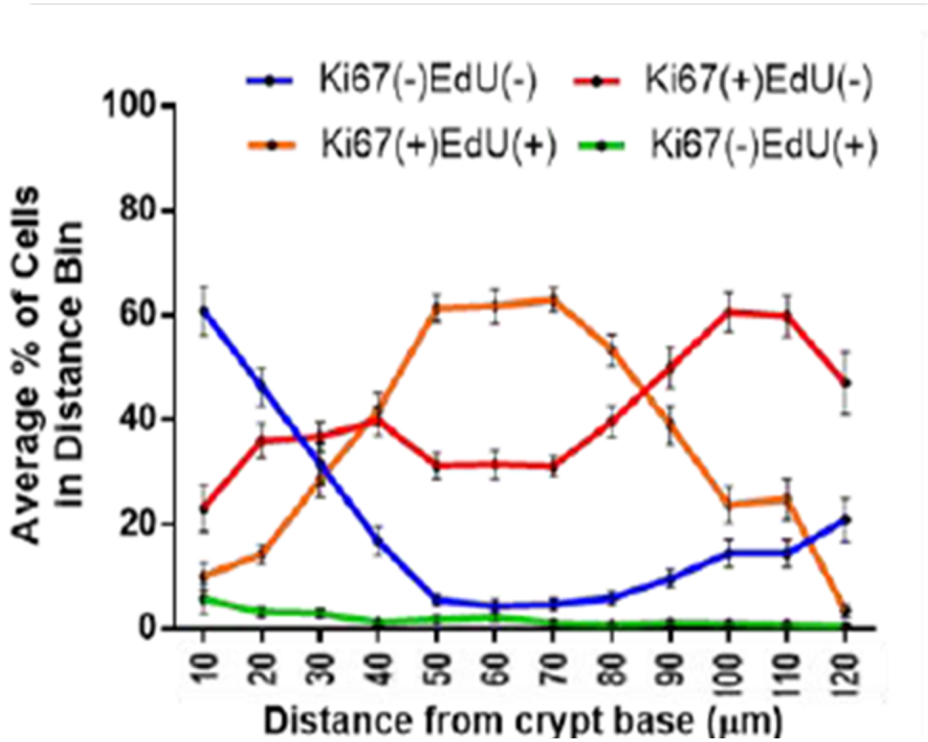


Carroll et al., S3 Figure

A

B

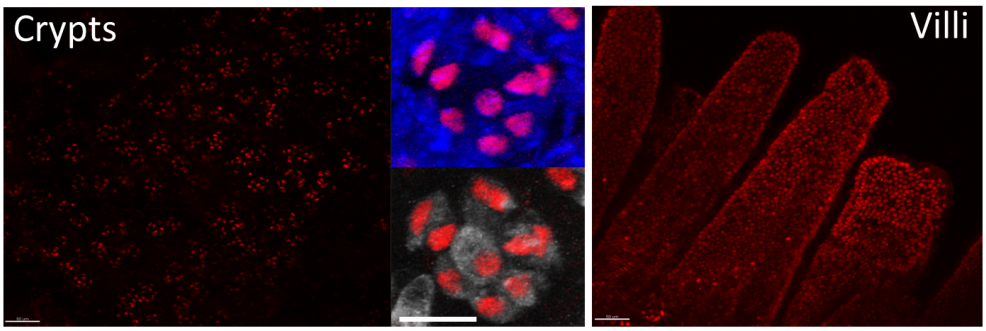


Nuclei hCdt1(30/120) Lysozyme

hCdt1(30/120)

C

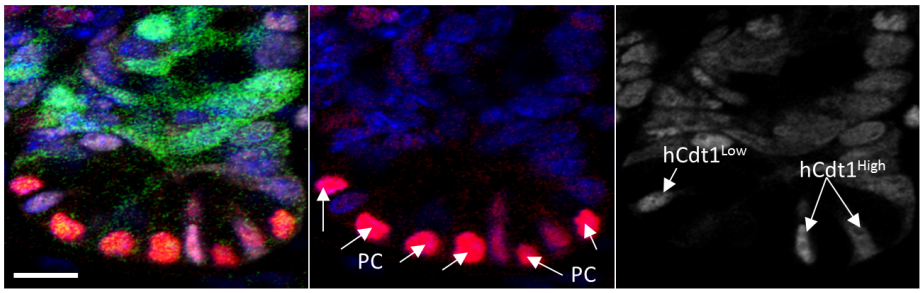


Nuclei hCdt1(30/120) hGem(1/110) Mcm2

D

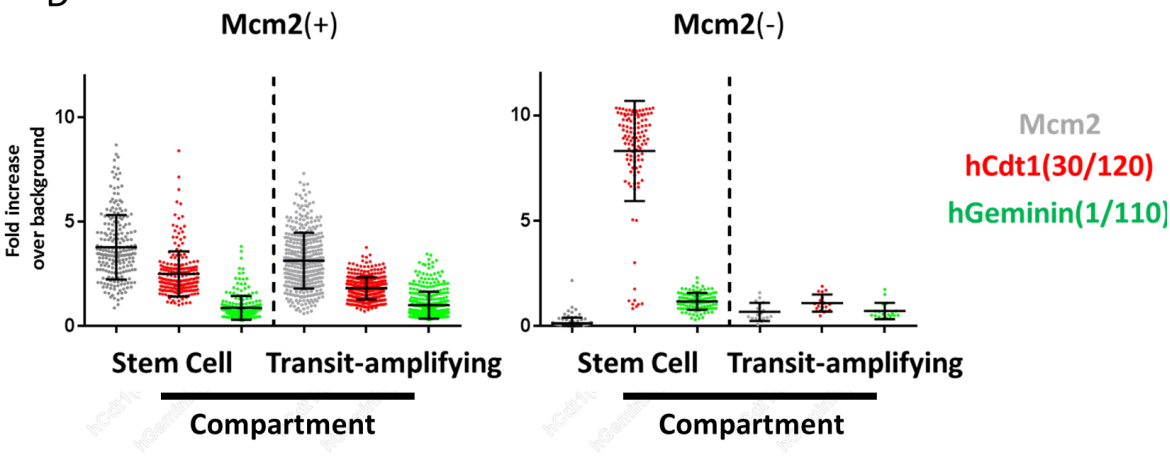

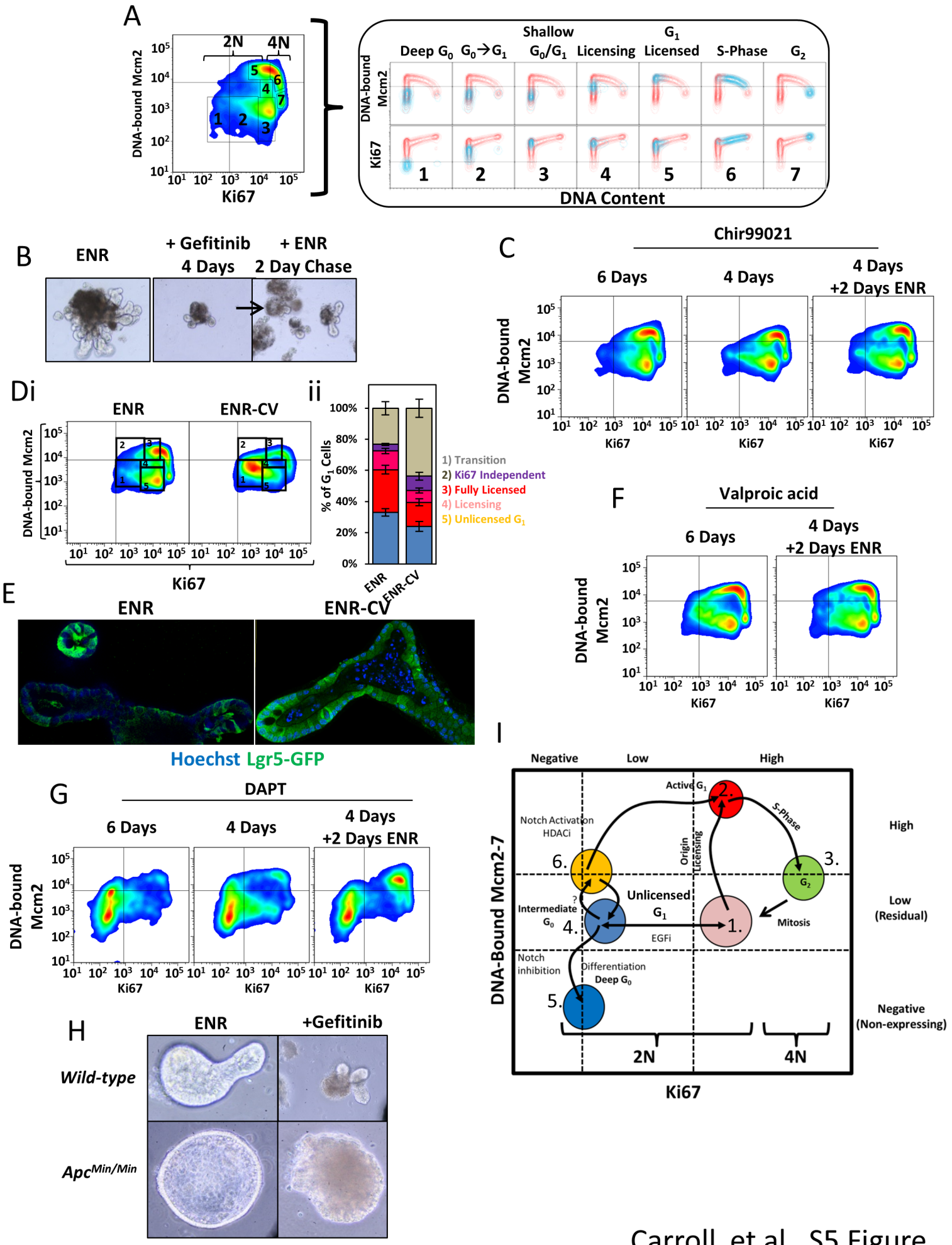


Carroll et al., S5 Figure